J. Fluid Mech. (2009), *vol.* 632, *pp.* 145–198.
doi:10.1017/S0022112009006958 Printed in the United Kingdom

Dynamics of dense sheared granular flows. Part II. The relative velocity distributions

V. KUMARAN†

Department of Chemical Engineering, Indian Institute of Science, Bangalore 560 012, India

(Received 10 May 2008 and in revised form 15 February 2009)

The distribution of relative velocities between colliding particles in shear flows of inelastic spheres is analysed in the volume fraction range 0.4–0.64. Particle interactions are considered to be due to instantaneous binary collisions, and the collision model has a normal coefficient of restitution e_n (negative of the ratio of the post- and pre-collisional relative velocities of the particles along the line joining the centres) and a tangential coefficient of restitution e_t (negative of the ratio of post- and pre-collisional velocities perpendicular to line joining the centres).

The distribution of pre-collisional normal relative velocities (along the line joining the centres of the particles) is found to be an exponential distribution for particles with low normal coefficient of restitution in the range 0.6–0.7. This is in contrast to the Gaussian distribution for the normal relative velocity in an elastic fluid in the absence of shear. A composite distribution function, which consists of an exponential and a Gaussian component, is proposed to span the range of inelasticities considered here. In the case of rough particles, the relative velocity tangential to the surfaces at contact is also evaluated, and it is found to be close to a Gaussian distribution even for highly inelastic particles.

Empirical relations are formulated for the relative velocity distribution. These are used to calculate the collisional contributions to the pressure, shear stress and the energy dissipation rate in a shear flow. The results of the calculation were found to be in quantitative agreement with simulation results, even for low coefficients of restitution for which the predictions obtained using the Enskog approximation are in error by an order of magnitude. The results are also applied to the flow down an inclined plane, to predict the angle of repose and the variation of the volume fraction with angle of inclination. These results are also found to be in quantitative agreement with previous simulations.

1. Introduction

The dynamics of a dense collection of sheared inelastic particles was analysed in Part I using event-driven simulations. Some of the salient results of that analysis, which have motivated the present more detailed analysis of the relative velocity distributions, are first discussed, and then the scope of the present analysis is outlined. First, we recall that for the shear flow of inelastic hard spheres, the dynamics of a binary collision depends on the normal and tangential coefficients of restitution, which are dimensionless, and the only time scale is the inverse of the strain rate. Therefore, the strain rate can be set equal to 1 without loss of generality in a homogeneous shear

† Email address for correspondence: kumaran@chemeng.iisc.ernet.in

flow. The mean square velocity and the angular velocity of the particles (granular temperatures) depend on the strain rate and the normal and tangential coefficients of restitution, e_n and e_t, through the energy balance condition. Therefore, the dynamics of the flow is completely determined by the volume fraction ϕ and the coefficients of restitution e_n and e_t. From dimensional analysis, it can be inferred that all components of the stress are proportional to $\dot{\gamma}^2$, while the rate of dissipation of energy is proportional to $\dot{\gamma}^3$, where $\dot{\gamma}$ is the strain rate. The Bagnold coefficients (ratio of the stress and $\dot{\gamma}^2$) and the scaled dissipation rate (dissipation rate scaled by $\dot{\gamma}^3$) are only functions of the volume fraction and coefficients of restitution.

In Part I, the ordering in a shear flow of inelastic particles was first analysed using both the in-plane and icosahedral bond orientational order parameters, denoted as q_6 and Q_6, respectively. For a gas of elastic spheres in the absence of shear, it should be recalled that the icosahedral order parameter Q_6 is close to zero for volume fraction $\phi < 0.49$. At $\phi = 0.49$, there is an ordering transition, and the bond orientational order parameter increases to a maximum value larger than 0.5. In contrast, for the shear flow of inelastic particles, it was shown in Part I that Q_6 is close to zero even at a volume fractions significantly larger than 0.49 if the system size is large enough. For a system with 500 particles in a cubic box at $e_n = 0.98$ and $e_t = 1$, it was observed that Q_6 is close to zero at volume fraction $\phi = 0.6$. For a lower coefficient of restitution $e_n = 0.6$, Q_6 was found to be close to zero at $\phi = 0.56$; simulations could not be carried out for higher volume fraction due to numerical errors. This indicates that the random state is the natural state for a sheared inelastic fluid in the limit of large system size, though ordering is induced when the system size is sufficiently small.

A second interesting result is that when there is no ordering (Q_6 is close to zero), particle motion is found to be diffusive, and the root mean square displacement of the particles is found to be proportional to time. However, when there is ordering, the root mean square displacement did not increase proportionally to time, and it was not possible to measure a diffusion coefficient. There was a sharp decrease in the diffusion coefficient at the onset of ordering. The diffusive motion of particles in the random state indicates that it is appropriate to treat the sheared inelastic material as a fluid, rather than as an anisotropic material in which ordered planes of particles slide past each other, or as a glassy material with diverging relaxation time. The diffusive motion is not isotropic, however, and the diffusion coefficient in the flow direction is larger than that in the other two directions. All off-diagonal components of the diffusion tensor were found to be zero within numerical accuracy.

The temperatures (mean square fluctuating velocities) were determined as a function of volume fraction and coefficient of restitution. It was found that the temperatures seem to approach a finite value as the close packing limit is approached, and the distribution of the fluctuating velocities is remarkably isotropic, with a variation of only about 20 % in the fluctuating translational and rotational energies in the different directions for $\phi > 0.5$.

An important finding of Part I: the collision frequency of particles showed a very sharp increase with volume fraction in the dense limit, and the collision frequency in a shear flow was much higher than that predicted for an elastic system at equilibrium (Torquato 1995). It is more common to write the collision frequency in terms of the pair distribution function in literature, but most of the relations are based on the assumption that the distribution of relative velocities is a Gaussian distribution. Therefore, in Part I, we preferred to work with the collision frequency itself. In the present paper, after analysing the distribution of relative velocities, we return and calculate the pair distribution function from the collision frequency. It was found, in

Part I, that the collision frequency for an inelastic shear flow diverges at a volume fraction lower than the random close packing volume fraction $\phi = 0.64$. For highly inelastic rough particles with e_n in the range 0.6–0.8, the collision frequency was found to diverge for a volume fraction of about $\phi_{ad} = 0.585$. Here, ϕ_{ad} is the volume fraction for arrested dynamics, where the collision frequency and stresses diverge at constant strain rate, or the strain rate goes to zero at constant stress. The form of the divergence was also found to be very different from that for an elastic fluid at the random close packing limit, where the pair distribution function increases as $(\phi_c - \phi)^{-1}$. Empirical correlations were proposed for the increase in the collision frequency with volume fraction near close packing.

The Bagnold coefficients (ratio of stress and $\dot{\gamma}^2$) and the scaled dissipation rate (ratio of stress and $\dot{\gamma}^3$) were found to increase proportionally to the collision frequency in the close packing limit. One of the approximations in the Enskog kinetic theory is that all collisional transfer rates, including the collision frequency, collisional stress and dissipation rates, increase proportionally to the pair distribution function, which diverges at the random close packing volume fraction. Therefore, the finding that the stress and dissipation rates increase proportionally to the collision frequency suggests that an important part of the Enskog approximation is valid. However, it was also found in Part I that the numerical agreement between the theory and simulation results is poor, even when the modified form of the collision frequency is incorporated into the theory. This suggests the failure of the molecular chaos assumption in the Enskog approximation, that the two-particle velocity distribution is the product of the single particle velocity distributions and the pair distribution function at contact. This implies that for inelastic systems, the correlations in the particle velocities alter the form of the distribution of relative velocities, and this results in a change in the collisional transport rates. In the present analysis, this aspect is analysed in detail, and we examine whether the inclusion of correlations in the relative velocity distribution can provide numerically accurate results for the stress and dissipation rate.

Since the shear flow is not isotropic, the distribution of relative velocities depends on the angle between the line joining the centres of the particles and the direction of flow. Therefore, the distribution of relative velocities is resolved into its spherical harmonic components, and it was found that in an expansion correct to second order in the strain rate there are only four non-zero components. These components are calculated from simulations, and the relations between these components and the pressure, dissipation rate, shear stress and normal stress differences are determined. For smooth particles, the relative velocity distribution in the direction along the line joining the centres can be used to calculate all components of the stress and the dissipation rate, since there is no impulse perpendicular to the line joining the centres at collision. In rough particles, only the shear stress depends on the impulse in the direction perpendicular to the line joining the centres, and we find that even this contribution is only about 10–20 % of the total shear stress. For rough particles, the distribution of velocities perpendicular to the line joining the centres is close to a Gaussian even at high volume fraction and low coefficient of restitution. However, we find that the distribution of velocities along the line joining the centres is very different from a Gaussian distribution.

The velocity distribution function for the pre-collisional relative velocity between particles is found to be an exponential distribution for both smooth and rough particles for coefficients of restitution in the range 0.6–0.8; we find that the variance of this distribution decreases to zero as the volume fraction ϕ_{ad} (where the collision

frequency diverges) is approached. We propose empirical forms for this distribution, and predict the dissipation rate and stresses using the empirical forms. Excellent agreement is found between predictions and the simulation results. This indicates that the dynamics of dense shear flows of inelastic particles can be successfully predicted by models based on the binary collision approximation, without the necessity of invoking correlations or coherent structures.

Collisions between particles are considered to be inelastic, and the normal coefficient of restitution e_n is less than 1, so that there is energy dissipation in the collisions. The collision models analysed include the smooth particle model, where the relative velocity tangential to the surfaces at contact is unchanged in a collision, as well as the rough particle model. In the rough particle model, we considered two cases, $e_t = 1$ where the relative tangential velocities of the surfaces at contact is exactly reversed in a collision, as well as $e_t = e_n$. In our analysis of the relative velocity distribution, we focus on the component of the relative velocity normal to the surfaces at contact, since this is the component which exhibits the maximum deviation from the Gaussian distribution for an elastic fluid. For rough inelastic particles, the dissipation of energy in a collision can be calculated from the normal relative velocity distribution only for $e_t = 1$; it would be necessary to model the tangential relative velocity distribution as well for the case $e_t < 1$ to calculate the energy dissipation. Since we restrict attention to the normal velocity distribution, we compare theory and simulations only for the case $e_t = 1$; a model for $e_t < 1$ would require additional fitting functions for the tangential velocity distributions which we do not analyse here. The comparison for $e_t = -1$ and $e_t = 1$ achieves the present objective of obtaining quantitative agreement between theory and simulations for all dynamical properties for a known collision model for a dense granular flow.

The theory and simulation results are also compared with an application of practical importance, which is the granular flow down an inclined plane. There are several remarkable features of the granular flow down an inclined plane which have been revealed by simulations (Silbert *et al.* 2001). It is observed that the volume fraction of the particles is a constant in the bulk of the flow, the granular temperature and all stress components are linear functions of height and the mean velocity increases as the square root of the height from the bottom of the layer. The lack of variation in the volume fraction was explained using kinetic theory (Kumaran 1998, 2006*a*, *b*, 2008), where the 'conduction length' $\delta = (d/(1 - e_n)^{1/2})$ was identified as the distance over which there is a balance between the rate of conduction of energy, and the rate of dissipation of energy due to inelastic collisions. Here, d is the particle diameter and e_n is the normal coefficient of restitution. When the thickness of the flowing layer h is large compared to the conduction length, the rate of conduction of energy can be neglected in the leading approximation, and the rate of production of energy due to mean shear is balanced by the rate of dissipation due to inelastic collisions. It has been shown that as a consequence of the balance between the rates of production and dissipation, the volume fraction is a constant in the leading approximation. The correction to the volume fraction is $O(\delta/h)^2$ smaller than the leading-order volume fraction. The variation of temperature and volume fraction in the boundary regions was analysed using boundary layer theory and matched asymptotic expansions in Kumaran (2008). An exact result was derived showing that a boundary layer solution is possible if and only if the volume fraction in the bulk decreases as the angle of inclination is increased. In addition, an expansion in the inverse of the pair distribution function was also used in the dense limit (where the pair distribution function is large) in order to obtain a single nonlinear differential equation for the

temperature profile. These results qualitatively reproduced the salient features of the flow down an inclined plane.

For the flow down an inclined plane, experiments (Pouliquen 1999) and simulations (Silbert *et al.* 2001) also show a steady flow is possible at a given angle of inclination only if the height of the layer is larger than a minimum height h_{stop}. While this height has been interpreted as a distance over which there are correlations in the flow (Ertas & Halsey 2002), the recent study of Kumaran (2008) showed that this could be explained on the basis of the dissipation of energy at the base. Analytical approximations were derived for the limits of small and large dissipation rates. The value of h_{stop} was calculated explicitly for different particle models, and the results are in qualitative agreement with experiments and simulations. Though all the features of the flow were reproduced qualitatively, the analysis of Kumaran (2008) indicated that there are quantitative differences between theory and simulations for the dependence of the volume fraction on the angle of inclination. The theory used for comparison was that of Kumaran (2006*a*) for rough and partially rough particles, in which the pair distribution function was assumed to be the same as that for elastic particles in the random close packing limit (Torquato 1995), and the Enskog approximation (two-particle velocity distribution is the product of the single-particle velocity distributions and the equilibrium pair distribution at contact) was used. The present analysis shows that these approximations are not valid for the shear flow of inelastic particles, and proposed alternate forms for the collision frequency (pair distribution function) and the distribution of relative velocities of colliding particles. Using these modified forms, we revisit the calculation of the stresses and the dependence of the angle of inclination on the volume fraction in the flow down an inclined plane. It is shown that quantitative agreement is obtained with these modifications.

2. Microscopic model and simulation technique

The system consists of rough inelastic spheres of diameter d subjected to a rate of deformation field $\mathbf{G} = \dot{\gamma}\boldsymbol{e}_x\boldsymbol{e}_y$. In the coordinate system used here, the flow is in the x direction, the velocity gradient in the y direction and the z coordinate is perpendicular to the flow plane, as shown in figure 1 of Part I. The particle mass m is set equal to 1 without loss of generality, so that all mass dimensions are non-dimensionalized by the particle mass. The ED simulation technique was already described in Part I. For completeness, we provide the microscopic collision model for the ED simulations. A rough particle collision model is used, in which the post-collisional relative velocity normal to the surfaces at contact is $-e_n$ times the pre-collisional normal relative velocity, and the post-collisional relative velocity tangential to the surfaces at contact is $-e_t$ times the pre-collisional relative tangential velocity. The normal coefficient of restitution e_n varies between 0 and 1; $e_n = 1$ corresponds to perfectly elastic collisions, while $e_n = 0$ corresponds to perfectly inelastic collisions. The tangential coefficient of restitution e_t varies between -1 and $+1$, $e_t = -1$ corresponds to smooth particles where there is no change in the relative velocity after collision, while $e_t = 1$ corresponds to perfectly rough particles where the relative velocity perpendicular to the line joining the centres is reversed after the collision. Energy is conserved for $e_n = 1$ and $e_t = \pm 1$.

There have been detailed measurements of binary collisions between particles (see, for example, Foerster *et al.* 1994) which show that the collision dynamics is more complicated than that assumed in the rough particle model. There are two types of collisions depending on the angle between the relative velocity vector and the line

joining the centres. Head-on collisions are found to be 'sticking' collisions, where the asperities on the particles lock during a collision. The impulse tangential to the colliding surfaces is proportional to the relative tangential velocity at the point of contact. Grazing collisions are found to be 'sliding' collisions, where the tangential impulse is equal to the coefficient of friction times the normal impulse. It is difficult to make quantitative comparisons with this collision model, because it is difficult to obtain constitutive relations for sliding collisions. It was possible to obtain results for a 'partially rough' collision model in earlier studies (Kumaran 2006*a*, 2008), where head-on collisions were considered rough, while grazing collisions were considered smooth. Here, we consider all collisions to be rough and characterized by just one normal and one tangential coefficients of restitution, in order to facilitate a quantitative comparison between theory and simulations. As explained in § 1, we have carried out simulations for rough particles for $e_t = -1$, $e_t = 1$ and $e_t = e_n$ for a range of normal coefficients of restitution. The comparison between analysis and simulations is restricted to $e_t = 1$ and $e_t = -1$, since this requires description of just the normal relative velocity distributions in collisions.

3. Two-particle velocity distribution function

Since we are interested in the collisional transport and dissipation of momentum and energy, we restrict our attention to particles in contact which are separated by one-particle diameter. We first carry out the analysis of the relative velocity distribution for rough particles; the results for smooth particles are a special case where the tangential velocity distribution and the angular velocity distribution are not relevant.

In a steady shear flow, it is necessary to define the two-particle velocity distribution function carefully, because the mean velocity $\mathbf{U}$ is a linear function of distance in the gradient direction. We consider two particles α and β with positions $\mathbf{x}_\alpha$ and $\mathbf{x}_\beta$, respectively. Without loss of generality, we can consider the mean velocity to be zero at the location $\mathbf{x}_\alpha$. In this case, the relative velocity distribution is a function of only the separation between the two particles, $\mathbf{x}_{\alpha\beta} = (\mathbf{x}_\alpha - \mathbf{x}_\beta)$, and does not depend on the absolute positions of the two particles. This assignment of zero mean velocity at the centre of particle α does not affect the stresses and dissipation rate. This is because the streaming stresses are related to the distribution of single-particle fluctuating velocities, and the collisional stresses are related to the distribution of relative velocities, while the rate of dissipation of energy is related only to the relative velocity distribution at contact.

The probability distribution that a particle α with position and velocity $(\mathbf{x}_\alpha, \mathbf{u}_\alpha, \omega_\alpha)$ is in contact with a second particle with position and velocity $(\mathbf{x}_\beta, \mathbf{u}_\beta, \omega_\beta)$, such that the unit vector from the centre of particle α to β is $\boldsymbol{k}$, is defined as $F(\mathbf{x}_\alpha, \mathbf{u}_\alpha, \omega_\alpha, \mathbf{u}_\beta, \omega_\beta, \boldsymbol{k})$. Here, $\mathbf{u}_\alpha$, $\mathbf{u}_\beta$, ω_α and ω_β are defined to be the pre-collisional velocities of the particles. Note that in a steady homogeneous shear flow, if the mean velocity $\mathbf{U}$ is zero at $\mathbf{x}_\alpha$, this function is independent of the location $\mathbf{x}_\alpha$ and time, and so we do not specify these in the following analysis. The two-particle distribution function for particles in contact can be used to determine the collision frequency, the collisional stresses and the rate of dissipation of energy. Before proceeding to define these transfer rates, it is useful to effect a change of variables from the particle velocities to the centre of mass velocity

$$\mathbf{v} = (\mathbf{u}_\alpha + \mathbf{u}_\beta)/2 \tag{3.1}$$

and the velocity difference

$$\boldsymbol{w} = (\mathbf{u}_\alpha - \mathbf{u}_\beta) \tag{3.2}$$

In a similar manner, the angular velocities of the two particles at contact can also be written in terms of the sum of the two angular velocities,

$$\boldsymbol{\varpi} = \omega_\alpha + \omega_\beta \tag{3.3}$$

and one half of the difference in angular velocities,

$$\upsilon = (\omega_\alpha - \omega_\beta)/2 \tag{3.4}$$

It can be easily verified that the Jacobians for these two transformations is 1.

The collisional impulse is independent of the velocity of the centre of mass **v**, and the difference between the angular velocities, υ. Therefore, we can define a reduced distribution function, which is the integral of the total distribution function over the centre of mass velocity and the difference in angular velocities for a pair of colliding particles.

$$f(\boldsymbol{w}, \boldsymbol{\varpi}, \boldsymbol{k}) = \int \mathrm{d}\mathbf{v} \int \mathrm{d}\upsilon F(\mathbf{u}_\alpha, \mathbf{u}_\beta, \omega_\alpha, \omega_\beta, \boldsymbol{k}) \tag{3.5}$$

For future reference, we also define the reduced distributions $f_w(\boldsymbol{w}, \boldsymbol{k})$ and $f_{\boldsymbol{\varpi}}(\boldsymbol{\varpi}, \boldsymbol{k})$ for the relative velocity and angular velocity, respectively,

$$f_w(\boldsymbol{w}, \boldsymbol{k}) = \int \mathrm{d}\boldsymbol{\varpi}\, f(\boldsymbol{w}, \boldsymbol{\varpi}, \boldsymbol{k}), \tag{3.6}$$

$$f_{\boldsymbol{\varpi}}(\boldsymbol{\varpi}, \boldsymbol{k}) = \int \mathrm{d}\boldsymbol{w} f(\boldsymbol{w}, \boldsymbol{\varpi}, \boldsymbol{k}). \tag{3.7}$$

A further reduction can be carried out to express the relative velocity in terms of its components along and perpendicular to the line joining the centres of the particles. For this purpose, we define

$$w_n = \boldsymbol{w} \cdot \boldsymbol{k} \tag{3.8}$$

$$\boldsymbol{w}_t = (\mathbf{I} - \boldsymbol{k}\boldsymbol{k}) \cdot \boldsymbol{w} \tag{3.9}$$

$$\boldsymbol{\varpi}_n = \boldsymbol{\varpi} \cdot \boldsymbol{k} \tag{3.10}$$

$$\boldsymbol{\varpi}_t = (\mathbf{I} - \boldsymbol{k}\boldsymbol{k}) \cdot \boldsymbol{\varpi} \tag{3.11}$$

Here, the unit vector $\boldsymbol{k}$ along the line joining the centres of the particles is defined as

$$\boldsymbol{k} = \sin(\theta)\cos(\phi)\boldsymbol{e}_x + \sin(\theta)\sin(\phi)\boldsymbol{e}_y + \cos(\theta)\boldsymbol{e}_z, \tag{3.12}$$

where $\boldsymbol{e}_x$, $\boldsymbol{e}_y$ and $\boldsymbol{e}_z$ are the unit vectors along the three-coordinate directions. The reduced distributions for each of these velocity components can be written as

$$f_{wn}(w_n, \boldsymbol{k}) = \int \mathrm{d}\boldsymbol{\varpi} \int \mathrm{d}\boldsymbol{w}_t f(\boldsymbol{w}, \boldsymbol{\varpi}, \boldsymbol{k}), \tag{3.13}$$

$$f_{wt}(\boldsymbol{w}_t, \boldsymbol{k}) = \int \mathrm{d}\boldsymbol{\varpi} \int \mathrm{d}w_n f(\boldsymbol{w}, \boldsymbol{\varpi}, \boldsymbol{k}), \tag{3.14}$$

$$f_{\boldsymbol{\varpi}n}(\boldsymbol{\varpi}_n, \boldsymbol{k}) = \int \mathrm{d}\boldsymbol{\varpi}_n \int \mathrm{d}\boldsymbol{w} f(\boldsymbol{w}, \boldsymbol{\varpi}, \boldsymbol{k}), \tag{3.15}$$

$$f_{\boldsymbol{\varpi}t}(\boldsymbol{\varpi}_t, \boldsymbol{k}) = \int \mathrm{d}\boldsymbol{\varpi}_n \int \mathrm{d}\boldsymbol{w} f(\boldsymbol{w}, \boldsymbol{\varpi}, \boldsymbol{k}). \tag{3.16}$$

Here, the integrals over $\mathrm{d}\boldsymbol{w}_t$ and $\mathrm{d}\boldsymbol{\varpi}_t$ are two-dimensional integrals over two independent components of the vectors $\boldsymbol{w}_t$ and $\boldsymbol{\varpi}_t$. It should be noted that the angular velocity in the direction of the line joining the centres, $\boldsymbol{\varpi}_n$, does not affect the collisional impulses, and therefore we do not consider the distribution of $\boldsymbol{\varpi}_n$ in the following analysis.

Since the anisotropy in the distribution function is generated due to the mean shear, the anisotropy has to be a function of the invariant components of the mean strain rate tensor G_{ij}, which are the symmetric part $S_{ij} = (G_{ij} + G_{ji})/2$ and the antisymmetric part $A_{ij} = (G_{ij} - G_{ji})/2$. This dependence is incorporated by defining a set of basis functions which are the spherical harmonics of the unit vector $\boldsymbol{k}$. The spherical harmonics are usually defined as

$$Y_{l,m}(\theta, \phi) = \sqrt{\frac{(2l+1)}{4\pi}\frac{(l-m)!}{(l+m)!}} P_l^m(\cos(\theta)) \exp(\imath m\phi) \tag{3.17}$$

where the index m can vary between $-l$ and $+l$, $P_l^m(\cos(\theta))$ are the Legendre polynomials, the azimuthal angle θ is the angle between the unit vector $\boldsymbol{k}$ and the z axis, and the meridional angle ϕ is the angle between the projection of the unit vector $\boldsymbol{k}$ on the x–y plane and the x axis. The spherical harmonics are orthonormal

$$\int_0^{2\pi} \mathrm{d}\phi \int_0^{\pi} \mathrm{d}\theta \, \sin(\theta) Y_{l,m}(\theta, \phi) Y_{pq}^*(\theta, \phi) = \delta_{lp}\delta_{mq}, \tag{3.18}$$

where the superscript * represents the complex conjugate.

Rather than using the complex spherical harmonics as the basis functions, it is more convenient to separate them into their real and imaginary parts, so that the entire analysis is carried out on the real axis. This is facilitated by the relationship between the real and imaginary parts of $Y_{l,m}$ and $Y_{l,-m}$, which is of the form $Y_{l,-m}(\theta, \phi) = (-1)^m Y_{l,m}^*(\theta, \phi)$. Due to this relationship, the real and imaginary parts of $Y_{l,m}(\theta, \phi)$ for $0 \leqslant m \leqslant l$ can also be used as the basis functions. We use the following basis functions, which provide the only non-zero contributions to the collision frequency, pressure, shear stress and normal stress differences:

$$\left.\begin{aligned} X_0(\theta, \phi) &= 1, \\ X_1(\theta, \phi) &= \frac{1}{4}\sqrt{\frac{15}{\pi}} \sin(\theta)^2 \sin(2\phi), \\ X_2(\theta, \phi) &= \frac{1}{4}\sqrt{\frac{5}{\pi}} (3\cos(\theta)^2 - 1), \\ X_3(\theta, \phi) &= \frac{1}{4}\sqrt{\frac{15}{\pi}} \sin(\theta)^2 \cos(2\phi). \end{aligned}\right\} \tag{3.19}$$

These basis functions are orthogonal with respect to integrations over the solid angle $\boldsymbol{k}$,

$$\int \mathrm{d}\boldsymbol{k} X_i(\boldsymbol{k}) X_j(\boldsymbol{k}) = N_i \delta_{ij}, \tag{3.20}$$

where the normalization constant $N_0 = 4\pi$, while the other normalization constants are all equal to 1. The distribution function is expanded in a series in the basis functions $X^{(i)}(\theta, \phi)$,

$$f^{(i)}(\boldsymbol{w}, \boldsymbol{\varpi}) = N_i^{-1} \int \mathrm{d}\boldsymbol{k} f(\boldsymbol{w}, \boldsymbol{\varpi}, \boldsymbol{k}) X_i(\boldsymbol{k}). \tag{3.21}$$

The distribution function can be reconstructed from its individual components,

$$f(\boldsymbol{w}, \boldsymbol{\varpi}, \boldsymbol{k}) = \sum_{i=0}^{3} f^{(i)}(\boldsymbol{w}, \boldsymbol{\varpi}) X_i(\boldsymbol{k}). \tag{3.22}$$

In expansion (3.22), we have included all spherical harmonics $Y_{lm}(\theta, \phi)$ (3.17) with $l = 0$ and $l = 2$. It is easy to see, from symmetries, that the coefficients of the terms with $l = 1$ are zero for a linear shear flow. The series has been truncated at $l = 2$, because all the dynamical quantities of interest in the present analysis, the collision frequency (3.61), the dissipation rate (3.60), the pressure (3.67), the shear stress due the normal impulse at collision (3.69) and the normal stress differences ((3.73) and (3.74)) can be evaluated from these components. There are no contributions to these dynamical quantities from the spherical harmonic components with $l \geqslant 3$.

In the simulations, the distribution function is obtained by first calculating the frequency of collisions between two particles with a relative normal or tangential velocity in the interval $\mathrm{d}\boldsymbol{w}\mathrm{d}\,\boldsymbol{\varpi}$ about $(\boldsymbol{w}, \boldsymbol{\varpi})$. It should be noted that collisions occur only when w_n is positive, while particles are moving away from each other when w_n is negative. Since the magnitude of the relative velocities before and after collision are different, the procedure for calculating the distribution function from the collision frequency is different from that for elastic systems, and we discuss this briefly.

The collision frequency, which is a function of the relative velocity and the angle of the line joining the centres of the particles at the point of collision, is expanded in a series in the spherical harmonics,

$$\nu(\boldsymbol{w}, \boldsymbol{\varpi}, \boldsymbol{k}) = \sum_{i=0}^{3} \nu_i(\boldsymbol{w}, \boldsymbol{\varpi}) X_i(\boldsymbol{k}), \tag{3.23}$$

where the functions $\nu_i(\boldsymbol{w}, \boldsymbol{\varpi})$ can be calculated from the collision frequency as follows:

$$\nu_i(\boldsymbol{w}, \boldsymbol{\varpi}) = \frac{1}{N_i} \int \mathrm{d}\boldsymbol{k}\; \nu(\boldsymbol{w}, \boldsymbol{\varpi}, \boldsymbol{k}) X_i(\boldsymbol{k}). \tag{3.24}$$

In the simulations, the individual functions ν_i are determined by summing up the functions X_i over all collisions with relative linear and angular velocities in the interval $\mathrm{d}\,\boldsymbol{w}$ about $\boldsymbol{w}$, and $\mathrm{d}\boldsymbol{\varpi}$ about $\boldsymbol{\varpi}$.

$$\nu_i(\boldsymbol{w}, \boldsymbol{\varpi})\mathrm{d}\boldsymbol{w}\;\mathrm{d}\boldsymbol{\varpi} = \frac{1}{\tau} \sum_{\text{collisions}} X_i(\boldsymbol{k}), \tag{3.25}$$

where τ is the total time period of the simulation. In the above expressions, the summation is carried out only over collisions with relative velocities in the interval $\mathrm{d}\boldsymbol{w}$ about $\boldsymbol{w}$, and $\mathrm{d}\boldsymbol{\varpi}$ about $\boldsymbol{\varpi}$. In order to obtain ν_i as a function of $\boldsymbol{w}$ and $\boldsymbol{\varpi}$ in the simulations, we use a binning procedure as follows. For the normal velocity w_n, the interval $0 \leqslant (w_n/\sqrt{2T}) \leqslant 5$ is divided into 50 intervals of width 0.1 each, and all collisions which occur within an interval are assigned to the velocity at the mid-point of the interval. Here, and in the following analysis, T is the translational temperature. In a similar manner, for the tangential velocity $\boldsymbol{w}_t$ and the component of the angular velocity tangential to the surface $\boldsymbol{\varpi}_t$, the intervals $0 \leqslant (|\boldsymbol{w}_t|/\sqrt{2T}) \leqslant 5$ and $0 \leqslant (|\boldsymbol{\varpi}_t|/\sqrt{2T/I}) \leqslant 5$ are divided into 50 intervals of width 0.1 each, and all collisions which occur within an interval are assigned to the mid-point of that interval. In this manner, we obtain the dependence of the collision frequency on the

relative velocity and angular velocity, and then extract the distribution functions for the relative velocity and angular velocity as discussed below.

The collision frequency can be related to the two-particle velocity distribution function as follows. First, we note that collisions occur only when the component of the relative velocity along the line joining the centres, w_n, is positive. In the dilute (point particle) limit, the frequency of collisions per unit volume between particles with relative velocity $(\boldsymbol{w}, \boldsymbol{\varpi})$ and relative orientation $\boldsymbol{k}$ can be written as

$$\nu(\boldsymbol{w}, \boldsymbol{\varpi}, \boldsymbol{k})\, \mathrm{d}\boldsymbol{w}\ \mathrm{d}\boldsymbol{\varpi}\ \mathrm{d}\boldsymbol{k} = \frac{\rho^2}{2} f(\boldsymbol{w}, \boldsymbol{\varpi}, \boldsymbol{k})\, w_n\, \mathrm{d}\boldsymbol{w}\, \mathrm{d}\boldsymbol{\varpi}\, \mathrm{d}\boldsymbol{k}, \tag{3.26}$$

where the factor (1/2) accounts for the fact that two particles are involved in a collision. In a dilute gas of hard particles, the single-particle distribution function is a Gaussian, the two-particle distribution is the product of the single-particle distributions, and the collision frequency can be evaluated by integrating (3.26) over velocities $\boldsymbol{w}$ and $\boldsymbol{\varpi}$, and the relative orientation of the line joining the centres with the relative velocity $\boldsymbol{k}$. We should note here that while calculating the collision frequency from (3.26), the relative velocity w_n should be integrated only in the domain $0 \leqslant w_n \leqslant \infty$, because collisions take place only when the relative velocity is positive. Using the Gaussian relative velocity distribution, and integrating over $\boldsymbol{w}$, $\boldsymbol{\varpi}$ and $\boldsymbol{k}$, we obtain the collision frequency as $2\rho^2\sqrt{\pi T}$, which is the standard expression in kinetic theory of gases (Chapman & Cowling 1970). For dense gases, the frequency of collision is larger than that predicted by (3.26), because the particles occupy a finite volume and due to the shadow effect, which increases the collision frequency. In this case, the collision frequency is written as

$$\nu(\boldsymbol{w}, \boldsymbol{\varpi}, \boldsymbol{k})\, \mathrm{d}\boldsymbol{w}\ \mathrm{d}\boldsymbol{\varpi}\ \mathrm{d}\boldsymbol{k} = \frac{\rho^2 \chi}{2} f(\boldsymbol{w}, \boldsymbol{\varpi}, \boldsymbol{k})\, w_n\, \mathrm{d}\boldsymbol{w}\, \mathrm{d}\boldsymbol{\varpi}\, \mathrm{d}\boldsymbol{k}. \tag{3.27}$$

Equation (3.27) defines the pair distribution function at contact, χ, when the relative velocity distribution function is defined to be normalized. Since the relative velocity distribution depends on the angle of the line joining the centres of the particles at collisions, represented by the unit vector $\boldsymbol{k}$, the normalization condition has to be represented as

$$\int \mathrm{d}\boldsymbol{k} \int \mathrm{d}\boldsymbol{w} \int \mathrm{d}\boldsymbol{\varpi}\, f(\boldsymbol{w}, \boldsymbol{\varpi}, \boldsymbol{k}) = 4\pi, \tag{3.28}$$

where the factor 4π accounts for the integration over the solid angle $\boldsymbol{k}$. This is equivalent to assuming that the isotropic component of the relative velocity distribution function, $f^{(0)}$, is normalized

$$\int \mathrm{d}\boldsymbol{w} \int \mathrm{d}\boldsymbol{\varpi}\, f^{(0)}(\boldsymbol{w}, \boldsymbol{\varpi}) = 1, \tag{3.29}$$

where the above integral is carried out over both positive and negative values of w_n. This serves to remove any ambiguity in the definition of the pair distribution function from (3.27). Defined this way, the pair distribution function at contact is a function of the volume fraction and the coefficient of restitution. The total collision frequency is obtained using an integral over the relative velocity distribution and the solid

angle $\boldsymbol{k}$,

$$\begin{aligned}\nu &= \frac{\rho^2\chi}{2}\int \mathrm{d}\boldsymbol{w}\int \mathrm{d}\boldsymbol{\varpi}\int \mathrm{d}\boldsymbol{k}\, f(\boldsymbol{w},\boldsymbol{\varpi},\boldsymbol{k})w_n \\ &= \frac{\rho^2\chi}{2}\left(\int_0^\infty \mathrm{d}w_n f^{(0)}_{w_n} w_n\right)\left(\int \mathrm{d}\boldsymbol{k} X_0(\boldsymbol{k})\right) \\ &= 2\pi\rho^2\chi\int_0^\infty \mathrm{d}w_n\, w_n\, f^{(0)}_{w_n}. \end{aligned} \tag{3.30}$$

The distribution function for particles with negative w_n (moving away from each other) is obtained from that for positive w_n (approaching each other) using the flux balance condition

$$f(\boldsymbol{w}',\boldsymbol{\varpi}',\boldsymbol{k})w_n'\mathrm{d}\boldsymbol{w}'\,\mathrm{d}\boldsymbol{\varpi}' = f(\boldsymbol{w},\boldsymbol{\varpi},\boldsymbol{k})w_n\mathrm{d}\boldsymbol{w}\,\mathrm{d}\boldsymbol{\varpi}. \tag{3.31}$$

Since $w_n' = -e_n w_n$, for $w_n < 0$, the Jacobian for transformation $(\boldsymbol{w}_t, \boldsymbol{\varpi})$ to $(\boldsymbol{w}_t', \boldsymbol{\varpi}')$ is 1 for $e_t = \pm 1$, we find the relation between the distribution functions to be

$$f(\boldsymbol{w}',\boldsymbol{\varpi}',\boldsymbol{k}) = e_n^{-2} f(\boldsymbol{w},\boldsymbol{\varpi},\boldsymbol{k}). \tag{3.32}$$

Using normalization condition (3.29), we find that the integral for positive relative velocities is given by

$$\int_0^\infty \mathrm{d}w_n \int \mathrm{d}\boldsymbol{w}_t \int \mathrm{d}\boldsymbol{\varpi}\int \mathrm{d}\boldsymbol{k}\, f(\boldsymbol{w},\boldsymbol{\varpi}) = \frac{4\pi}{1+e_n^{-1}}. \tag{3.33}$$

Using the above condition, pair distribution function is related to the collision frequency by

$$\begin{aligned}\chi &= \frac{(1+e_n^{-1})}{2}\int \mathrm{d}\boldsymbol{k}\int_0^\infty \mathrm{d}w_n\,(\nu(w_n,\boldsymbol{k})/(\rho^2 w_n)) \\ &= 2\pi(1+e_n^{-1})\int_0^\infty \mathrm{d}w_n\,(\nu_0(w_n)/\rho^2 w_n). \end{aligned} \tag{3.34}$$

The distribution function for the relative velocity for $w_n > 0$ is then given by (3.27) while the relative velocity distribution for $w_n < 0$ is given by (3.32). In a similar manner, the terms in the spherical harmonic expansion (3.24) for the relative velocity distribution are given by

$$f^{(i)}(\boldsymbol{w},\boldsymbol{\varpi}) = \frac{2\nu^{(i)}(\boldsymbol{w},\boldsymbol{\varpi})}{\rho^2\chi\, w_n} \tag{3.35}$$

for $w_n > 0$. We first analyse the velocity distribution functions, obtained from the collision frequency using (3.27), and then return to properties such as the pair distribution function, dissipation rate and the stresses.

The distribution of the pre-collisional velocity along the line joining the centres, $f^{(0)}_{wn}(w_n)$, is shown as a function of w_n for a linear shear flow with volume fraction $\nu = 0.56$ and for different values of the coefficient of restitution in figure 1 for smooth particles, and in figure 2 for rough particles. An important observation is that the qualitative nature of the relative velocity distribution is the same for both smooth and rough particles. When the particles are nearly elastic ($e_n = 0.98$), the relative velocity distribution is close to a Gaussian, and mean square of the relative velocity distribution is actually more than two times the translational temperature. However, as the coefficient of restitution decreases, the velocity distribution deviates significantly from a Gaussian distribution, and approaches an exponential distribution

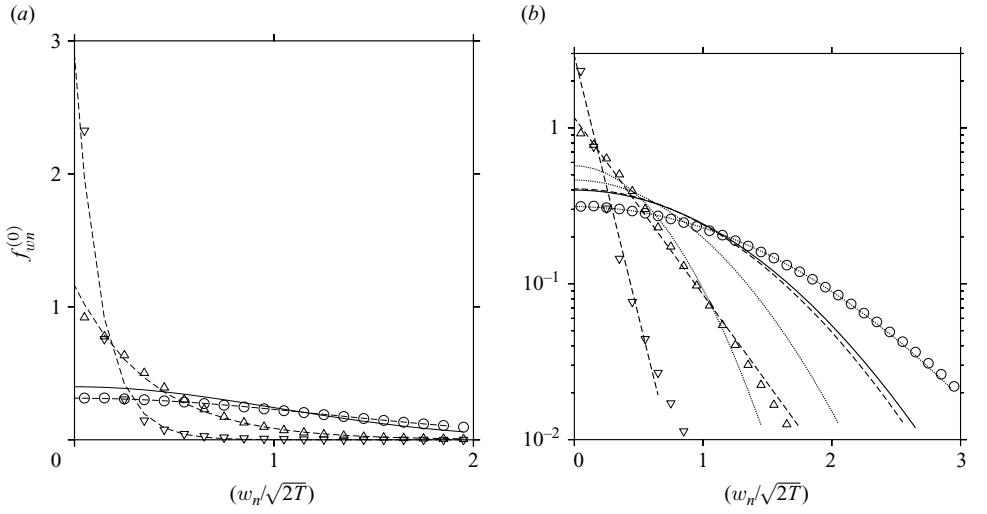

FIGURE 1. The relative velocity distribution $f^{(0)}_{w_n}$ as a function of the scaled relative velocity $(w_n/\sqrt{2T})$ for $\nu = 0.56$, for smooth particles ($e_t = -1$), and for normal coefficients of restitution $e_n = 0.98$ ($\circ$), $e_n = 0.8$ ($\triangle$) and $e_n = 0.6$ (∇). (*a*) The distribution function on a linear scale and (*b*) the same distribution on a semi-log scale. The dotted lines show the best Gaussian fit, the dashed line is the composite distribution function (3.40) and the solid line is the Gaussian distribution function for an elastic system.

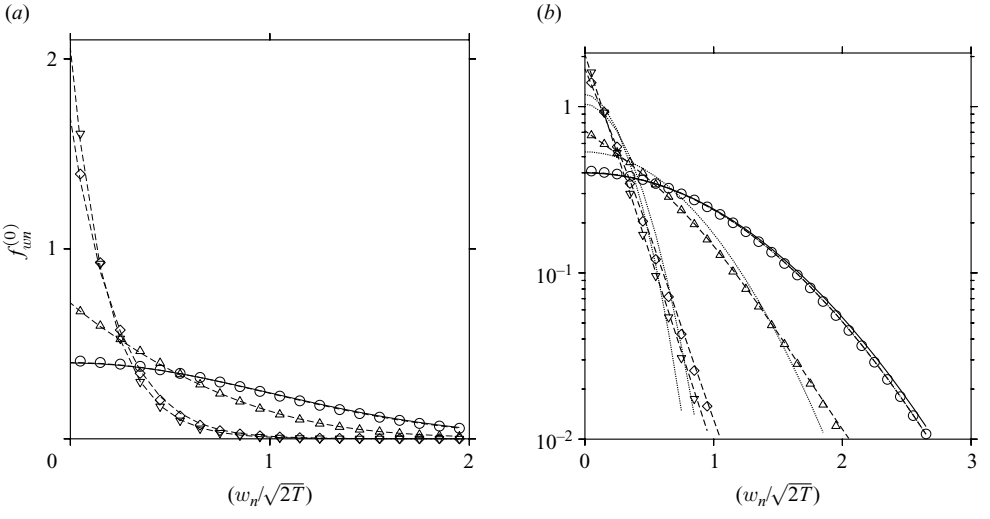

FIGURE 2. The relative velocity distribution $f^{(0)}_{w_n}$ as a function of the scaled relative velocity $(w_n/\sqrt{2T})$ for $\nu = 0.56$, for rough particles for coefficients of restitution $e_n = 0.98$, $e_t = 1.0$ ($\circ$); $e_n = 0.8$, $e_t = 1.0$ ($\triangle$); $e_n = 0.6$, $e_t = 1.0$ (∇); and $e_n = 0.8$, $e_t = 0.8$ ($\diamond$). (*a*) The distribution function on a linear scale and (*b*) the same distribution on a semi-log scale. The dashed lines are the best fits to the composite distribution function (3.40), the dotted lines show the best Gaussian fit and the solid line is the Gaussian distribution function for an elastic system.

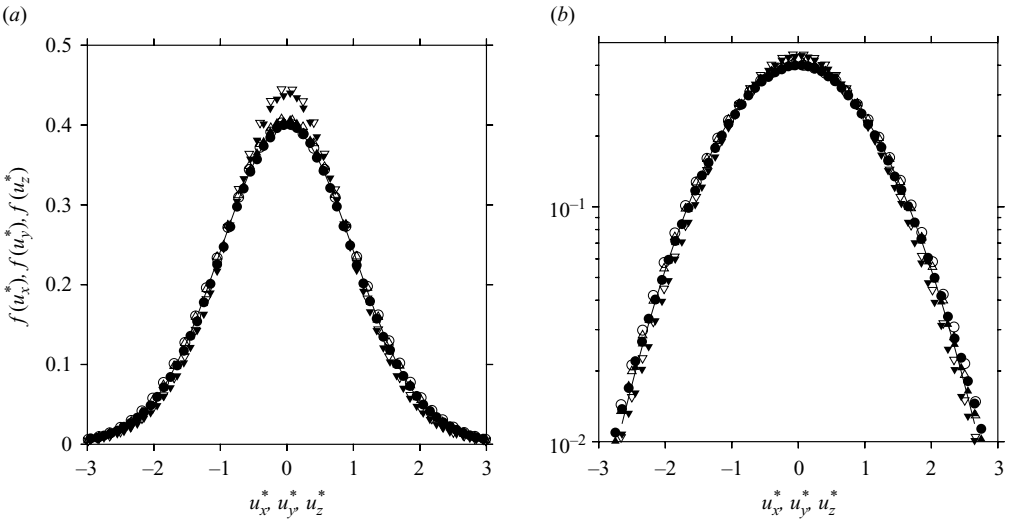

FIGURE 3. The velocity distributions $f(u_x^*)$ (○), $f(u_y^*)$ (△) and $f(u_z^*)$ (∇) as a function of the scaled velocities $(u_x^* = u_x/\sqrt{T}), (u_y^* = u_y/\sqrt{T})$ and $u_z^* = (u_z/\sqrt{T})$ for $\phi = 0.56$ and $e_n = 0.6$. The solid symbols show the results for rough particles $e_t = 1.0$, and the open symbols show the results for smooth particles $e_t = -1.0$. The solid line is the Gaussian distribution function for an elastic system.

at a coefficient of restitution of 0.6, while the distribution function is intermediate between an exponential and a Gaussian at $e_n = 0.8$. It is observed from figure 1 that for $e_n = 0.98$, the decay is slower than the best Gaussian fit in the limit of large velocities. The fourth standardized moment (ratio of fourth moment and square of second moment) for this distribution is larger than that for a Gaussian distribution, and therefore the Gaussian distribution does not provide a good fit. In addition, even the composite distribution (3.40) does not provide a good fit for the distribution function at $e_n = 0.98$. This is because the composite distribution is designed to model the transition from a Gaussian to an exponential distribution, which involves a reduction in the fourth standardized moment, and therefore it cannot capture an increase in the fourth standardized moment. In a similar manner, for $e_n = 0.6$, there is a deviation from the exponential form at high velocities, and the best fit seems to be either a smaller exponent or slower than exponential decay. However, we do not observe this deviation for rough particles. This is an interesting feature which deserves closer examination, but this does not significantly alter the results. This is because the distribution function decreases rapidly at large velocities, and a difference in the form of the velocity distribution in the large velocity limit does not significantly alter the predictions for the stresses and dissipation rates.

It should be noted that even though the distribution function for the velocity of approach deviates significantly from a Gaussian, the distribution function for the particle velocities does not show a similar deviation. Figure 3 shows the distribution function for the actual particle velocities for $e_n = 0.6$ and the volume fraction $\phi = 0.56$, for both rough and smooth particles. It is observed that the distribution function for rough particles is quantitatively close to a Gaussian even at high volume fraction and low coefficient of restitution. This indicates that the departure of the distribution function for the relative velocity from the Gaussian form is not because the single-particle velocity distributions are distorted, but rather because of the correlation in

the velocities of the neighbouring particles. So this effect cannot be captured by altering the single-particle velocity distribution; it is necessary to have a model for the distribution of relative velocities between pairs of particles.

In order to describe the functional form of the distribution function for the relative velocity both for nearly elastic and for highly inelastic systems, it is necessary to accommodate both the exponential and Gaussian forms of the distribution function. The Gaussian distribution function for the pre-collisional relative velocity for $w_n > 0$ is given by

$$f_{wn}^{(0)}(w_n) = \frac{1}{\sqrt{\pi T_{wn}/2}\left(1 + e_n^{-1}\right)} \exp\left(-w_n^2/2T_{wn}\right). \tag{3.36}$$

The post-collisional relative velocity (for $w_n < 0$) can be obtained from the pre-collisional relative velocity using a flux balance condition for the colliding particles

$$f_{wn}^{(0)}(w_n) = \frac{1}{\sqrt{\pi T_{wn}/2}\left(1 + e_n^{-1}\right)e_n^2} \exp\left(-w_n^2/2e_n^2 T_{wn}\right). \tag{3.37}$$

It should be noted that T_{wn} is defined to be the temperature for the pre-collisional velocities in (3.36); the temperature for the post-collisional velocities is (T_{wn}/e_n^2). In a similar manner, if the distribution function is an exponential distribution, then the distribution for the pre-collisional velocity has the form

$$f_{wn}^{(0)}(w_n) = \frac{\alpha}{1 + e_n^{-1}} \exp\left(-\alpha w_n\right), \tag{3.38}$$

where the parameter α is obtained from the exponential decay of the distribution function. The post-collisional relative velocity distribution for $w_n < 0$ is then given by

$$f_{wn}^{(0)}(w_n) = \frac{\alpha}{e_n^2\left(1 + e_n^{-1}\right)} \exp\left(-\alpha w_n/e_n\right). \tag{3.39}$$

Once again, the parameter α is calculated from the standard deviation for the pre-collisional velocity.

In order to account for the transition from a Gaussian to an exponential distribution, we define a composite distribution function for the velocity which accommodates both the exponential and the Gaussian forms. Since the stresses and dissipation rate can be calculated from the distribution of pre-collisional velocities, it is necessary to propose a composite distribution only for the pre-collisional velocities. This composite distribution is of the form

$$f_{wn}^{(0)}(w_n) = \frac{C}{1 + e_n^{-1}}\alpha \exp\left(-\alpha w_n\right) + \frac{(1 - C)}{\sqrt{\pi T_{wn}/2}\left(1 + e_n^{-1}\right)} \exp\left(-w_n^2/2T_{wn}\right), \tag{3.40}$$

where the parameter α is calculated from the distribution function obtained by the simulations using

$$\alpha = \left(\frac{6\int_0^\infty \mathrm{d}w_n\, w_n^3\, f_{wn}^{(0)}(w_n)}{\int_0^\infty \mathrm{d}w_n\, w_n\, f_{wn}^{(0)}(w_n)}\right)^{-1/2} \tag{3.41}$$

and T_{wn}, the effective temperature for the normal velocity fluctuations and the translational temperature is given by

$$T_{wn} = \left(\frac{2\int_0^\infty \mathrm{d}w_n\, w_n^3\, f_{wn}^{(0)}(w_n)}{\int_0^\infty \mathrm{d}w_n\, w_n\, f_{wn}^{(0)}(w_n)}\right) = \frac{3}{\alpha^2}. \tag{3.42}$$

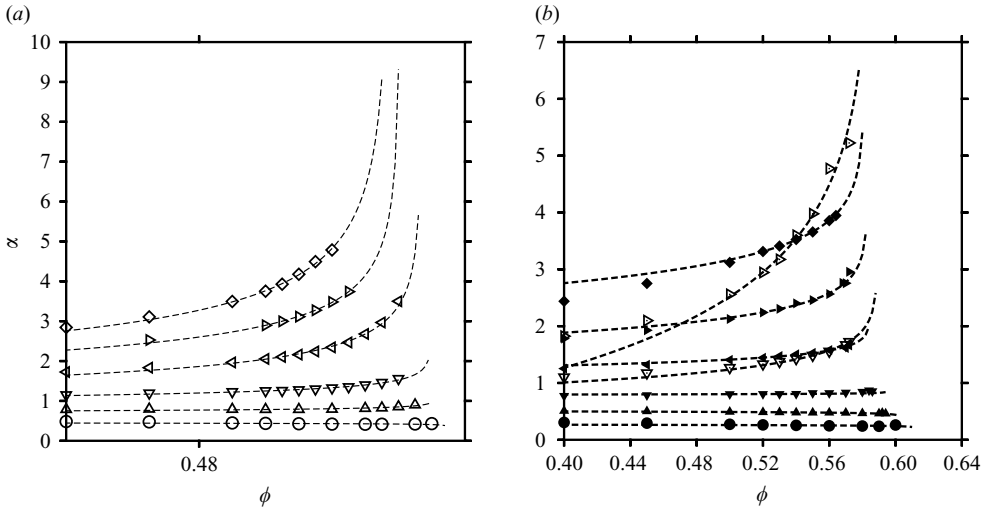

FIGURE 4. The parameter α in the normal velocity distribution (3.40) for $e_n = 0.98$ ($\bigcirc$), $e_n = 0.95$ ($\triangle$), $e_n = 0.9$ (∇), $e_n = 0.8$ ($\triangleleft$), $e_n = 0.7$ ($\triangleright$), $e_n = 0.6$ ($\diamond$), and for (*a*) smooth particles $e_t = -1.0$ (open symbols) and (*b*) $e_t = 1.0$ (filled symbols) and $e_t = e_n$ (open symbols with inscribed dots). The dashed lines show fits (3.45) and (3.46).

The constant C in (3.40) is a fitted parameter, which is obtained by minimizing the mean square of the deviation of the actual distribution from the composite distribution (3.40). The reasoning behind the above composite distribution is as follows. Since the distribution function is an exponential distribution for small values of the coefficient of restitution, it is expected that $C = 1$ in (3.40). In this case, it is easily verified that the parameter α is given by (3.41). If the distribution function is a Gaussian distribution at coefficients of restitution close to 1, the value of C in (3.40) will be small. In this case, the parameter T_{wn} is given by (3.42). The composite distribution, shown by the broken lines in figures 1 and 2, is in excellent agreement with the distribution function obtained from simulations for rough particles, even at the intermediate value of $e_n = 0.8$, at which neither the Gaussian nor the exponential distribution provides a good fit. For smooth nearly elastic particles $e_n = 0.98$, it is observed that the distribution function for the relative velocity is broader than the equivalent Gaussian distribution for elastic particles at the same translational temperature. This indicates that the effective temperature for the relative velocity distribution initially increases as the coefficient of restitution is reduced from 1. However, for lower values of the coefficient of restitution, the distribution function changes in form. For rough particles at $e_n = 0.6$, a single exponential decay provides an excellent fit. For smooth particles at $e_n = 0.6$, the distribution function has one exponential decay at low relative velocity, and a slower exponential decay in the high velocity limit. The composite distribution function (3.40) accurately captures the first exponential decay for smooth particles. The high velocity exponential decay is not accurately captured by the distribution function (3.40), but as explained earlier, the distribution function is numerically small in the high velocity region, and the error in this region does not significantly affect the stresses and the dissipation rates.

The parameters α and C are shown as a function of e_n for different volume fractions in figures 4 and 5. It is observed that C is close to 1 for $e_n = 0.6, 0.7$; it decreases to about 0.5 for $e_n = 0.8$, and is close to 0 for $e_n = 0.9$ and 0.95. This indicates a clear

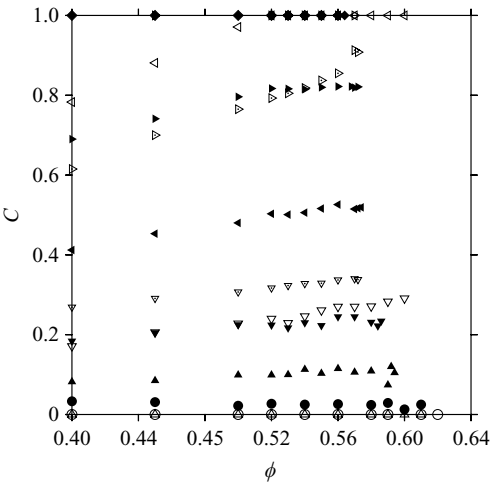

FIGURE 5. The constant C in distribution function (3.40) as a function of volume fraction at $e_n = 0.98$ (○), $e_n = 0.95$ (△), $e_n = 0.9$ (∇), $e_n = 0.8$ (◁), $e_n = 0.7$ (▷) and $e_n = 0.6$ (◇). The open symbols show the results for smooth particles ($e_t = -1$), while the filled symbols show the results for rough particles ($e_t = 1$), and the symbols with inscribed dots show the results for rough particles with $e_t = e_n$.

change in the nature of the distribution function from a Gaussian to an exponential form at about $e_n = 0.8$. An important observation from figure 5 is that the constant C, which provides the fractions of the exponential and Gaussian distributions in the composite distribution function (3.40), is nearly a constant with volume fraction in the range 0.52–0.58. The only exception is the value for smooth inelastic particles with $e_n = 0.8$ and rough inelastic particles with $e_t = 0.8$ and $e_n = 0.8$, for which C varies in the range 0.6–0.9 as the volume fraction is increased. For all other values, the variation in C is very small in the range 0.5 to ϕ_{max}, though there is a larger variation in the range 0.4–0.5. This can be used to advantage in arriving at a model for the distribution function in the dense limit. The average value of C in the range $\phi = 0.52$ to $\phi = \phi_{max}$ is shown in figure 6 for both smooth and rough particles. For rough particles, the fitting form

$$C = \begin{cases} 2.5(1 - e_n) & \text{for } e_n > 0.6 \\ 1.0 & \text{for } e_n < 0.6 \end{cases} \tag{3.43}$$

is in very good agreement with the data. In the case of smooth particles, we find that $C = 0$ for $e_n \geqslant 0.95$, and $C = 1$ for $e_n \leqslant 0.8$. There is only one intermediate point $e_n = 0.9$ at which C is about 0.26. More simulations in the range $0.8 \leqslant e_n \leqslant 0.95$ would be required to infer a functional form for C. Here, we use the form

$$C = \begin{cases} 0.0 & \text{for } e_n \geqslant 0.95 \\ 1.0 & \text{for } e_n \leqslant 0.8 \\ 0.26 & \text{for } e_n = 0.9. \end{cases} \tag{3.44}$$

As explained earlier, we do not attempt to model the case of rough particles with $e_t = e_n$, since this requires a detailed analysis of the relative tangential velocity distributions as well.

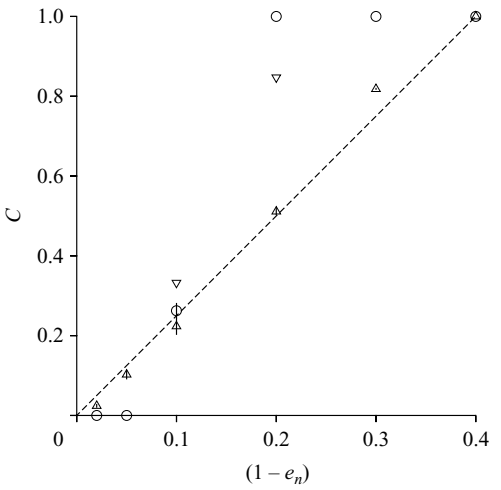

FIGURE 6. The average value of C in distribution function (3.40), averaged over the volume fraction range 0.52 to ϕ_{max}, as a function of e_n for rough particles ($e_t = 1$) (○), rough particles with $e_t = e_n$ (▽) and for smooth particles ($e_t = -1$) (△). The line shows fit (3.43).

Figure 4 provides an indication that the parameter α is diverging as the close packing limit is approached for coefficients of restitution between 0.6 and 0.8 for $e_t = 1$; this divergence is more clearly seen for $e_n = 0.8$ and $e_t = 0.8$. However, it should be cautioned that a definitive conclusion cannot be drawn because we do not have simulation results for volume fractions very close to ϕ_{ad}. As best as we can infer, the divergence is logarithmic for rough particles, and a power law for smooth particles. In the case of rough particles, the parameter α is found to be fitted best by a logarithmic relationship of the form

$$\alpha = A_\alpha \log(\phi_{ad} - \phi) + B_\alpha \tag{3.45}$$

while for smooth particles, the best fit is found to be of the form

$$\alpha = B_\alpha(\phi_{ad} - \phi)^{A_\alpha}, \tag{3.46}$$

where the parameters A_α and B_α are provided in table 1. The best fits, obtained using (3.45) and (3.46), and the parameters in table 1, are shown by the dotted lines in figure 4.

It should be noted that both of the divergences in (3.45) and (3.46) are weak in comparison to the divergence of the collision frequency in (3.25) in Part I. Therefore, these do not qualitatively alter the dynamics of the flow in the close packing limit or the divergence of the stresses in the close packing limit. However, the divergence of α has two consequences, one intuitively expected and the second puzzling. The divergence of α near the close packing limit indicates that the distribution function of relative velocities between particles is tending to a delta function around $w_n = 0$ in the close packing limit; this is intuitively expected, since the delta function at zero relative velocity represents the stoppage of flow at close packing. However, the divergence would result in a violation of the energy balance relation. This is because the shear stress is proportional to the second moment of the relative velocity distribution, and so the shear production of energy (at constant strain rate) diverges as α^{-2} for an exponential distribution. In contrast, the rate of dissipation of energy is proportional to the third moment of the relative velocity distribution, and so the rate of dissipation

	Rough particles			Smooth particles: $e_n = -1.0$		
e_n	e_t	A_α	B_α	e_n	A_α	B_α
0.98	1.0	0.0085	0.2781	0.98	−0.0280	0.4637
0.95	1.0	0.0121	0.5163	0.95	−0.0528	0.6950
0.90	1.0	−0.0178	0.7643	0.90	−0.1237	0.9402
0.80	1.0	−0.2049	1.2258	0.80	−0.2642	1.0961
0.70	1.0	−0.4860	1.1721	0.70	−0.2659	1.4842
0.60	1.0	−0.5400	1.8013	0.60	−0.3254	1.6200
0.90	0.90	−0.3005	0.5086			
0.80	0.80	−1.6100	1.4500			

TABLE 1. The parameters A_α and B_α in (3.45) and (3.46) for the parameter α as a function of the coefficient of restitution and the volume fraction.

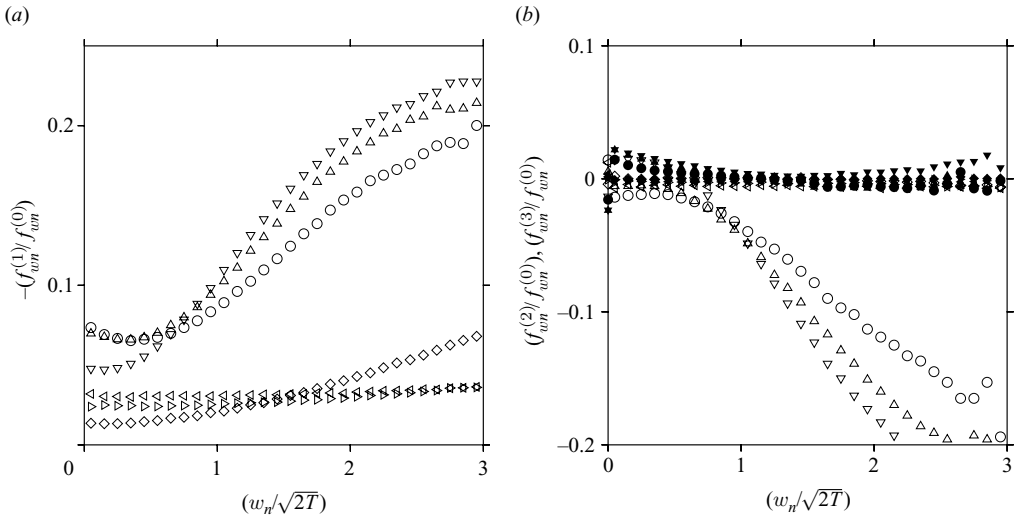

FIGURE 7. The ratios $-(f_{wn}^{(1)}/f_{wn}^{(0)})$ (*a*), $(f_{wn}^{(2)}/f_{wn}^{(0)})$ and $(f_{wn}^{(3)}/f_{wn}^{(0)})$ (*b*), as a function of $(w_n/2\sqrt{T})$, for different volume fractions and coefficients of restitution for smooth particles with $e_t = -1$, ($\circ$) $e_n = 0.6, \phi = 0.56$; ($\triangle$) $e_n = 0.6, \phi = 0.52$; (∇) $e_n = 0.6, \phi = 0.4$; ($\triangleleft$) $e_n = 0.98, \phi = 0.58$; ($\triangleright$) $e_n = 0.98, \phi = 0.52$; ($\diamond$) $e_n = 0.98, \phi = 0.4$. In (*b*), the open symbols show $(f_{wn}^{(2)}/f_{wn}^{(0)})$ and the filled symbols show $(f_{wn}^{(3)}/f_{wn}^{(0)})$.

diverges as α^{-3}. A balance between these cannot be achieved in the limit $\alpha \to \infty$, even if the divergence is only logarithmic. This could indicate that there is a true divergence which is cutoff for some reason; it is also possible that there is no true divergence and (3.45) and (3.46) are a consequence of our inability to get close enough to the close packing volume fraction. More detailed simulations or theoretical investigations are required to resolve this issue.

Next, we turn to the components of the distribution function in the spherical harmonic expansion, $f_{wn}^{(1)}$, $f_{wn}^{(2)}$ and $f_{wn}^{(3)}$, which are not spherically symmetric. Instead of analysing the distributions themselves, it proves more profitable to analyse the ratio of these components with the isotropic distribution function $f_{wn}^{(0)}$, which are referred to as the distribution ratios. These are shown in figure 7 for smooth particles, and in figure 8 for rough particles. First, we examine the variation of the distribution

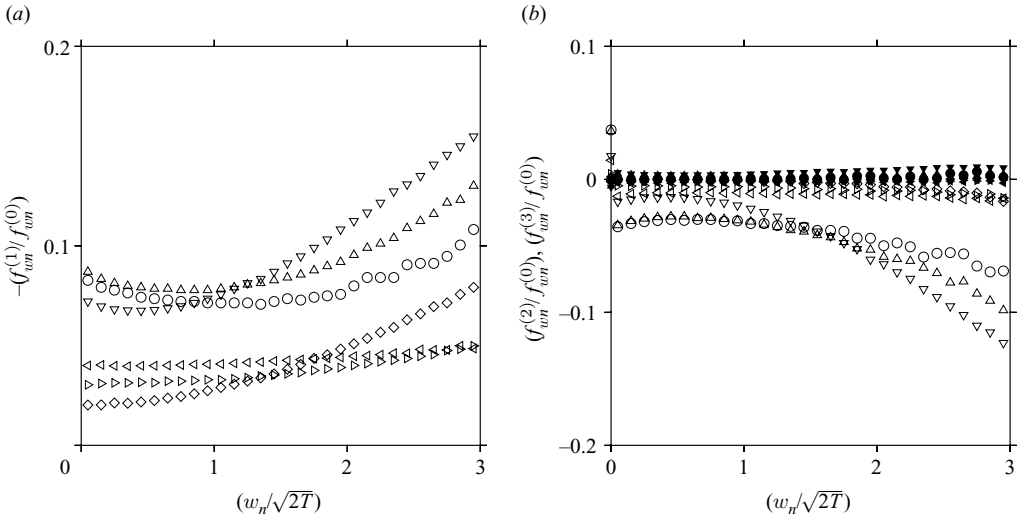

FIGURE 8. The ratios $-(f_{wn}^{(1)}/f_{wn}^{(0)})$ (*a*), $(f_{wn}^{(2)}/f_{wn}^{(0)})$ and $(f_{wn}^{(3)}/f_{wn}^{(0)})$ (*b*), as a function of $(w_n/2\sqrt{T})$, for different volume fractions and coefficients of restitution for rough particles with $e_t = 1$, ($\circ$) $e_n = 0.6, \phi = 0.56$; ($\triangle$) $e_n = 0.6, \phi = 0.52$; (∇) $e_n = 0.6, \phi = 0.4$; ($\triangleleft$) $e_n = 0.98, \phi = 0.58$; ($\triangleright$) $e_n = 0.98, \phi = 0.52$; ($\diamond$) $e_n = 0.98, \phi = 0.4$. In (*b*), the open symbols show $(f_{wn}^{(2)}/f_{wn}^{(0)})$ and the filled symbols show $(f_{wn}^{(3)}/f_{wn}^{(0)})$.

ratios with volume fraction. It is evident that the ratios $(f_{wn}^{(1)}/f_{wn}^{(0)})$, $(f_{wn}^{(2)}/f_{wn}^{(0)})$ and $(f_{wn}^{(3)}/f_{wn}^{(0)})$ are nearly independent of volume fraction in the volume fraction range between 0.52 and ϕ_{max}, even though the collision frequency is increasing by 1–2 orders of magnitude in this range. There is a change in the form of the distribution ratios when the volume fraction is further reduced to 0.4. This indicates that all the components of the distribution function in a spherical harmonic expansion are evolving in a self-similar manner as the volume fraction is changed in the dense limit.

The distribution ratios for nearly elastic particles are nearly independent of the relative velocity w_n in the dense limit. This is surprising, and in contradiction to the results based on the Enskog approximation for dense gases, where the two-particle distribution function is written as

$$f^{(2)}(\mathbf{x}, \mathbf{x}', \mathbf{u}, \mathbf{u}') = \chi(\phi) f(\mathbf{x}, \mathbf{u}) f(\mathbf{x}', \mathbf{u}'), \tag{3.47}$$

where $\chi(\phi)$ is the pair distribution function which is a function of the volume fraction ϕ, $\mathbf{x}' = \mathbf{x} + \boldsymbol{k}$, where $\boldsymbol{k}$ is the unit vector along the line joining the centres of the particles (the particle diameter is considered to be 1 in the present analysis). Figure 3 shows that at high volume fraction and low coefficient of restitution, the single-particle velocity distribution is remarkably close to a Gaussian distribution. In addition, the distribution of velocities is nearly isotropic. The same is not true at lower volume fractions, where the shear has a significant effect on the single-particle velocity distribution (Lutsko 1996; Garzo & Dufty 1999). Consider the single-particle velocity distribution, consistent with figure 3, to be a Gaussian function of the fluctuating velocity

$$f(\mathbf{x}, \mathbf{u}) = \frac{1}{(2\pi T)^{3/2}} \exp\left(-(\mathbf{u} - \mathbf{G}\cdot\mathbf{x})^2/2T\right), \tag{3.48}$$

where $\mathbf{u}$ is the absolute particle velocity, and $\mathbf{G}\cdot\mathbf{x}$ is the mean velocity at the location $\mathbf{x}$, where $\mathbf{G}$ is the strain rate. Substituting this into the equation for the pair distribution function, we obtain,

$$f^{(2)}(\mathbf{x}, \mathbf{x}', \mathbf{u}, \mathbf{u}') = \chi(\phi) f_v(\mathbf{v}) f_w(\boldsymbol{w}), \tag{3.49}$$

where $\mathbf{v} = (\mathbf{u} + \mathbf{u}')/2$ is the velocity of the centre of mass, $\boldsymbol{w} = (\mathbf{u} - \mathbf{u}')$ is the velocity difference and the distribution functions f_v and f_w are

$$f_v(\mathbf{v}) = \frac{1}{(\pi T)^{3/2}} \exp\left(-(\mathbf{v} - \mathbf{G}\cdot(\mathbf{x} + \mathbf{x}')/2)^2/T\right), \tag{3.50}$$

$$f_w(\boldsymbol{w}) = \frac{1}{(4\pi T)^{3/2}} \exp\left(-(\boldsymbol{w} + \mathbf{G}\cdot(\mathbf{x} - \mathbf{x}'))^2/(4T)\right). \tag{3.51}$$

If the relative velocity distribution (3.51) is expanded in the strain rate $\mathbf{G}$, and only the term proportional to $\mathbf{G}$ is retained in the expansion, we obtain

$$f_w(\boldsymbol{w}) = \frac{1}{(4\pi T)^{3/2}} \exp\left(-\boldsymbol{w}^2/4T\right)\left(1 - \frac{\boldsymbol{w}\cdot\mathbf{G}\cdot\boldsymbol{k}}{2T}\right). \tag{3.52}$$

The normal velocity distribution is obtained by integrating (3.52) over the tangential velocities of the particles, to obtain

$$f_{wn}(w_n) = \frac{1}{(4\pi T)^{1/2}} \exp\left(-w_n^2/4T\right)\left(1 - \frac{w_n \boldsymbol{k}\cdot\mathbf{G}\cdot\boldsymbol{k}}{2T}\right). \tag{3.53}$$

The spherical harmonic component $f_{wn}^{(1)}$, obtained using (3.53), for a linear shear flow with $\mathbf{G} = \dot{\gamma}\boldsymbol{e}_x\boldsymbol{e}_y$, is

$$f_{wn}^{(1)} = -\sqrt{\frac{2\pi}{15}}\frac{w_n \exp\left(-\boldsymbol{w}^2/4T\right)}{(4\pi T)^{3/2}}. \tag{3.54}$$

Therefore, the Enskog approximation would predict that $(f_{wn}^{(1)}/f_{wn}^{(0)}) \propto w_n$ in the limit $w_n \ll 1$. Clearly, this approximation is not valid in the dense limit even for nearly elastic particles. Instead, we observe that the ratio of $f_{wn}^{(1)}$ and $f_{wn}^{(0)}$ is nearly independent of w_n. If a similar procedure was carried out to second order in $\mathbf{G}$, the Enskog approximation would predict that there are two contributions to $f_{wn}^{(2)}$ and $f_{wn}^{(3)}$, one of which is independent of w_n, while the other is quadratic in w_n. However, we observe that the ratios $(f_{wn}^{(2)}/f_{wn}^{(0)})$ and $(f_{wn}^{(3)}/f_{wn}^{(0)})$ are nearly independent of w_n for nearly elastic particles.

For inelastic particles with $e_n = 0.6$, the distribution function $f_{wn}^{(0)}$ decreases exponentially, and it decreases by more than an order of magnitude for $(w_n/\sqrt{2T}) = 1$. In this range, the distribution ratios are nearly independent of the relative velocity. A constant distribution ratio provides a significant simplification, because the higher moments of the distributions $f_{wn}^{(1)}$, $f_{wn}^{(2)}$ and $f_{wn}^{(3)}$ can be written as the products of the distribution ratio and the corresponding moments of $f_{wn}^{(0)}$. Since we already have an analytic form for the distribution function $f_{wn}^{(0)}$, this can be used to predict analytic forms for the other spherical harmonic components of the distribution function. These can then be used to provide predictions for the shear stress and the normal stress differences.

One possible approximation which could be made to relate $f_{wn}^{(1)}$ and $f_{wn}^{(0)}$ is to assume that the mean strain rate affinely advects the distribution function. In this case, the relative velocity distribution should be a function of $(\boldsymbol{w} - \mathbf{G}\cdot\boldsymbol{k})$ only, where $\boldsymbol{w} = (\mathbf{u}_\alpha - \mathbf{u}_\beta)$ is the difference in the absolute velocity of the two particles, and $(\boldsymbol{w} - \mathbf{G}\cdot\boldsymbol{k})$ is the difference in the fluctuating velocities. If the relative velocity

distribution function is an exponential distribution, the equivalent of (3.53) for a distribution function of the form (3.38), with $\boldsymbol{w}$ replaced by $(\boldsymbol{w} - \mathbf{G}\cdot\boldsymbol{k})$, is

$$f_{wn}(w_n) = \alpha \exp(-\alpha w_n)(1 - \alpha \boldsymbol{k}\cdot\mathbf{G}\cdot\boldsymbol{k}). \tag{3.55}$$

Using this, the ratio $(f_{wn}^{(1)}/f_{wn}^{(0)})$ is given by

$$\left(f_{wn}^{(1)}/f_{wn}^{(0)}\right) = 2\sqrt{\frac{2\pi}{15}}\alpha\dot{\gamma}. \tag{3.56}$$

We find that the above prediction is too high by more than an order of magnitude for all the cases studied here, leading us to conclude that we cannot approximate the distribution function by an isotropic exponential distribution affinely deformed by the mean shear.

There are two ways in which one could evaluate the constant distribution ratios. The first is to take the value in the limit of small w_n, where the distribution ratio is nearly a constant. However, this method has the drawback that the actual value obtained depends on the range of w_n over which the averaging is carried out. One could also define the distribution ratio as the ratios of the integrals of the distribution functions

$$\left.\begin{aligned} c_{wn}^{(1)} &= \frac{\int_0^\infty \mathrm{d}w_n f_{wn}^{(1)}}{\int_0^\infty \mathrm{d}w_n f_{wn}^{(0)}} \\ c_{wn}^{(2)} &= \frac{\int_0^\infty \mathrm{d}w_n f_{wn}^{(2)}}{\int_0^\infty \mathrm{d}w_n f_{wn}^{(0)}} \\ c_{wn}^{(3)} &= \frac{\int_0^\infty \mathrm{d}w_n f_{wn}^{(3)}}{\int_0^\infty \mathrm{d}w_n f_{wn}^{(0)}} \end{aligned}\right\} \tag{3.57}$$

This definition is advantageous because it is unambiguous. In addition, while carrying out the integrals, the regions where the distribution function have lower numerical values are given less weightage. The values of the ratios of the integrals of the distribution function are shown as a function of volume fraction for different coefficients of restitution in figure 9. It is observed that $c_{wn}^{(1)}$ is negative, and increases as the coefficient of restitution decreases. It is also observed that $c_{wn}^{(1)}$ is larger for rough particles than for smooth particles. The ratio $c_{wn}^{(2)}$ is mostly negative for the range of volume fractions and coefficients of restitution studied here, and is larger for rough particles. The ratio $c_{wn}^{(3)}$ is much smaller in magnitude than $c_{wn}^{(2)}$, and is negative in sign. These coefficients are used to calculate the shear stress and the normal stress differences a little later.

Before proceeding to use the relative velocity distribution to obtain the dissipation rate and the stress, we briefly examine the distribution of the tangential velocity and the angular velocity for rough particles in the dense limit. The tangential velocity distribution is not relevant for the dissipation rate and stresses for smooth particles, because there is no transmission of impulse in the direction tangential to the surface at contact. For rough particles, there is a transmission of impulse tangential to the surface at contact, and this leads to a non-zero contribution to the shear stress. The distributions for the pre-collisional velocity perpendicular to the line joining the centres, $f_{wt}^{(0)}(\mathbf{w}_t)$, and the sum of the pre-collisional angular velocities along the line joining the centres, $f_{\upsilon t}^{(0)}(\boldsymbol{\varpi}_t)$, are shown for rough particles at volume fraction $\phi = 0.56$ for different coefficients of restitution in figures 10 and 11. It is observed that the relative tangential velocity and the relative angular velocity are close to Gaussian distributions, though their variances differ from the expected value $2T$ for an elastic system. Also shown in figures 10 and 11 are the best Gaussian fits for the distribution

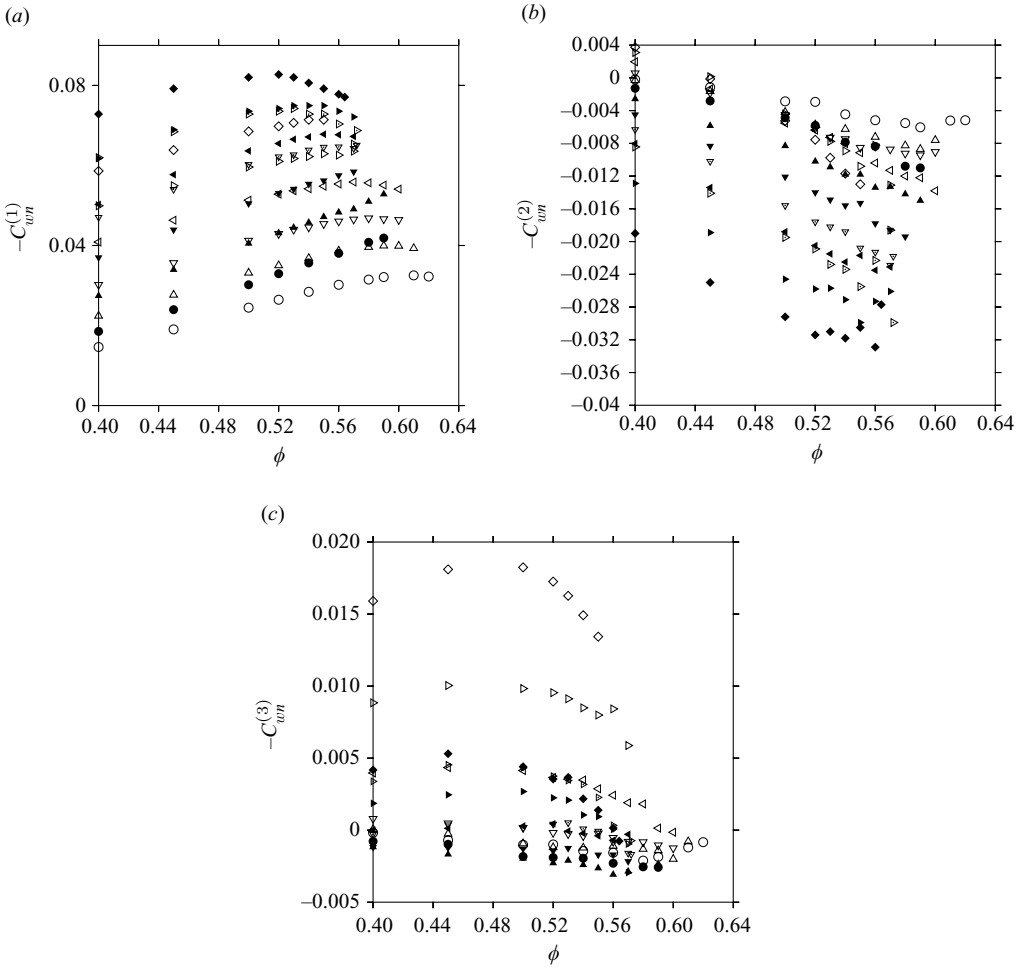

FIGURE 9. The ratios $-c_{wn}^{(1)}$ (*a*), $c_{wn}^{(2)}$ (*b*) and $c_{wn}^{(3)}$ (*c*), as a function of volume fraction ϕ, for different coefficients of restitution (○) $e_n = 0.98$, (△) $e_n = 0.95$, (▽) $e_n = 0.9$, (◁) $e_n = 0.8$, (▷) $e_n = 0.7$, (◇) $e_n = 0.6$. The open symbols show the results for smooth particle $e_t = -1$, and the filled symbols show the results for rough particles $e_t = 1$, and the open symbols with inscribed dots show the results for $e_t = e_n$.

functions. It is observed that the Gaussian fits for the relative tangential velocity $\mathbf{w}_t$ and the relative angular velocity $\boldsymbol{\varpi}_t$ are in good agreement with the distributions evaluated in simulations.

Next, we examine the deviation from the relative mean square velocities and angular velocities from the values for an elastic fluid by plotting $(\langle \mathbf{w}_t^2 \rangle / 2T)$ and $(\langle \mathscr{I} \boldsymbol{\varpi}_t^2 \rangle / 2T)$ in figure 12. As expected, these ratios are close to 1 for nearly elastic collisions, but deviate significantly from 1 as collisions are made more inelastic. Interestingly, it is observed that the mean square of the tangential relative velocity is larger than $2T$, though the maximum deviation is less than 10 % even for highly inelastic collisions with $e_n = 0.6$. The mean square of the relative angular velocity during a collision shows a larger deviation from $2T$, but the form of the distribution is still Gaussian, as shown in figure 12. It is observed that the effective temperature for the relative tangential velocity is quite close to the translational temperature even for $e_n = 0.6$,

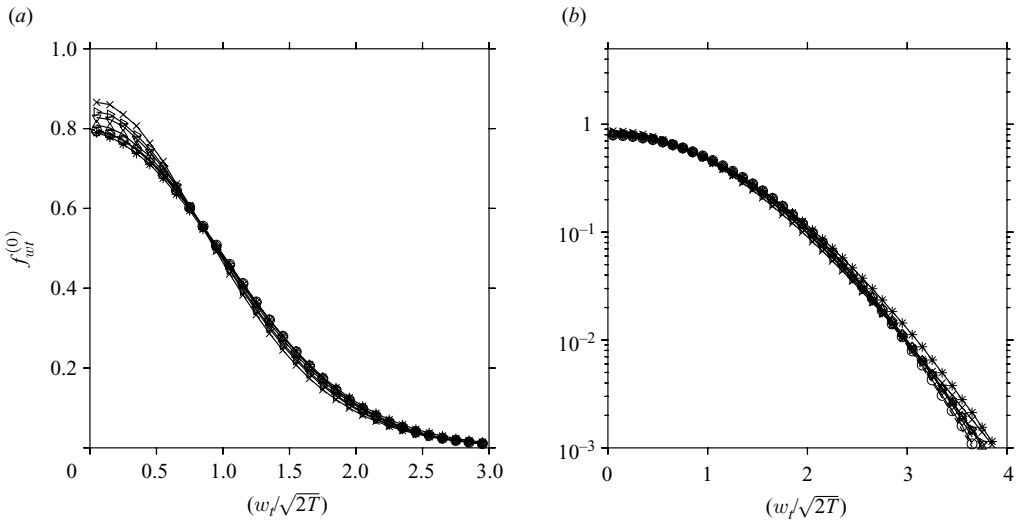

FIGURE 10. The relative velocity distribution $f_{wt}^{(0)}$ as a function of the scaled relative velocity $(w_t/\sqrt{2T})$ for $\nu = 0.56$, for coefficients of restitution $e_n = 0.95, e_t = 1.0$ ($\circ$); $e_n = 0.9, e_t = 1.0$ ($\diamond$); $e_n = 0.8, e_t = 1.0$ ($\triangle$); $e_n = 0.7, e_t = 1.0$ (∇); $e_n = 0.6, e_t = 1.0$ ($\triangleright$); $e_n = 0.9, e_t = 0.9$ ($*$); $e_n = 0.8, e_t = 0.8$ ($\times$). (*a*) The distribution function on a linear scale and (*b*) the same distribution on a semi-log scale. The dotted lines are the best Gaussian fits, and the broken line is the Gaussian distribution function for an elastic system.

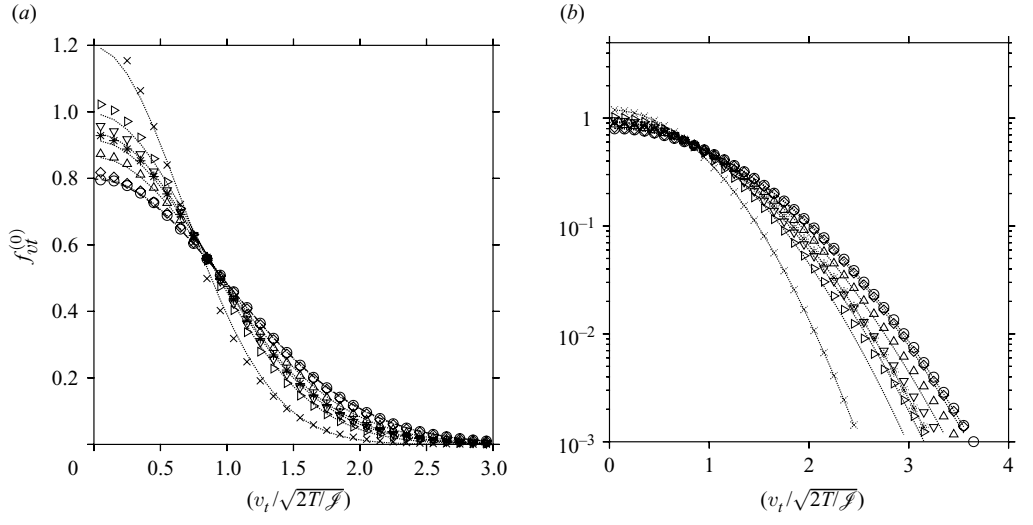

FIGURE 11. The relative angular velocity distribution $f_{vt}^{(0)}$ as a function of the scaled relative velocity $(v_t/\sqrt{2T/\mathscr{I}})$ for $\nu = 0.56$, and for coefficients of restitution $e_n = 0.98, e_t = 1.0$ ($\circ$); $e_n = 0.9, e_t = 1.0$ ($\diamond$); $e_n = 0.8, e_t = 1.0$ ($\triangle$); $e_n = 0.7, e_t = 1.0$ (∇); $e_n = 0.6, e_t = 1.0$ ($\triangleright$); $e_n = 0.9, e_t = 0.9$ ($*$); $e_n = 0.8, e_t = 0.8$ ($\times$). (*a*) The distribution function on a linear scale and (*b*) the same distribution on a semi-log scale. The dotted lines are the best Gaussian fits, and the broken line is the Gaussian distribution function for an elastic system.

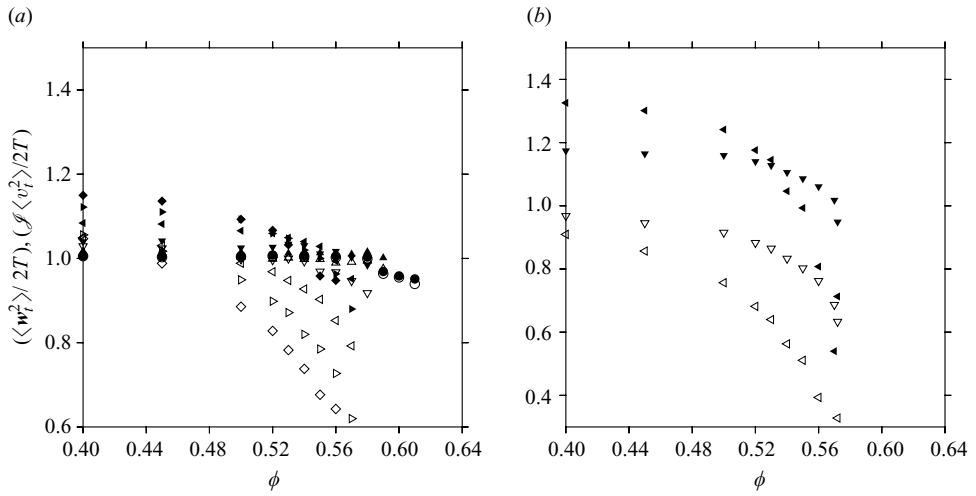

FIGURE 12. The mean square of the relative velocities scaled by two times the temperature, $(\langle \mathbf{w}_t^2 \rangle / 2T)$ (filled symbols) and $(\mathscr{I} \langle v_t^2 \rangle / 2T)$ (open symbols), as a function of the volume fraction for rough particles $e_t = 1.0$ (*a*) and $e_t = e_n$ (*b*), and with normal coefficients of restitution (○) $e_n = 0.98$; (△) $e_n = 0.95$; (▽) $e_n = 0.9$; (◁) $e_n = 0.8$; (▷) $e_n = 0.7$; (◇) $e_n = 0.6$.

while the effective temperature for the relative rotational velocity does decrease to a minimum of about 0.6 times the translational temperature. For the case of $e_t = e_n$, there is a significantly larger decrease in the ratio of the mean square of the relative angular velocity distribution, and the effective temperature for the relative rotational velocity decreases to about 0.3 times the translational temperature. This indicates that the rotational velocity fluctuations decrease faster than the relative translational velocity fluctuations as the coefficient of restitution is decreased, even though the distribution functions continue to be well approximated by a Gaussian distribution.

The pair distribution function, as calculated from (3.34) is compared with that obtained using the Gaussian distribution (3.36) for the relative velocity distribution and for elastic particles

$$\nu = \rho^2 \chi \sqrt{2\pi T_{wn}} = 2\rho^2 \chi \sqrt{\pi T} \tag{3.58}$$

in figures 13 and 14. Here, the temperature for the relative velocity distribution T_{wn} is two times the translational temperature for the particles. The pair distribution function calculated using the correction proposed by Garzo & Dufty (1999) differs by less than 2 % from that calculated using (3.58) in the present calculations, and so we do not plot this separately here. It is observed there is a large difference between the two results, which has a maximum of a factor of 4 for $e_n = 0.6$. The Gaussian approximation for the relative velocity (3.58) always underestimates the pair correlation function in all cases, except for smooth particles with $e_n = 0.98$. The over-estimation in the case of $e_n = 0.98$ for smooth particles is because the effective normal temperature is larger than the translational temperature of the particles. This indicates that (3.58), or the modified form of Garzo & Dufty (1999), is not a good approximation for the pair distribution function in the dense limit, and it is preferable to use a correlation for the collision frequency in the form of (3.34).

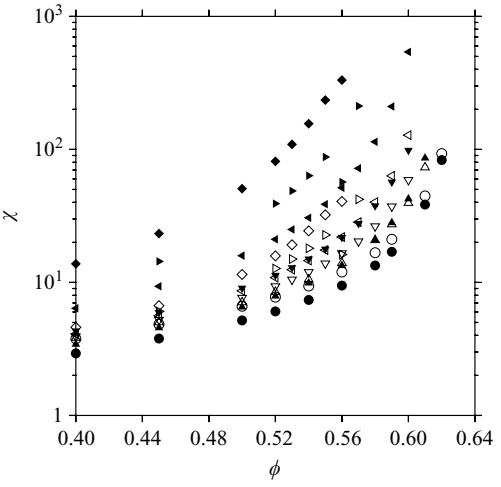

FIGURE 13. The pair distribution function χ as a function of the volume fraction ϕ for smooth particles with $e_t = -1$, and with normal coefficient of restitution $e_n = 0.98$ ($\circ$); $e_n = 0.95$ ($\triangle$); $e_n = 0.9$ (∇); $e_n = 0.8$ ($\triangleleft$); $e_n = 0.7$ ($\triangleright$); $e_n = 0.6$ ($\diamond$). The filled symbols show the results obtained using (3.34), while the open symbols show the result using a Gaussian distribution for the relative velocity distribution (3.58). The pair distribution function calculated using the correction proposed by Garzo & Dufty (1999) is indistinguishable from that calculated using (3.58).

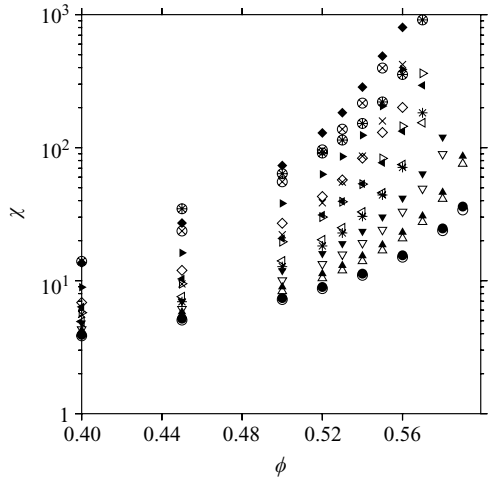

FIGURE 14. The pair distribution function χ as a function of the volume fraction ϕ for rough particles with coefficient of restitution $e_n = 0.98, e_t = 1.0$ ($\circ$); $e_n = 0.95, e_t = 1.0$ ($\triangle$); $e_n = 0.9, e_t = 1.0$ (∇); $e_n = 0.8, e_t = 1.0$ ($\triangleleft$); $e_n = 0.7, e_t = 1.0$ ($\triangleright$); $e_n = 0.6, e_t = 1.0$ ($\diamond$); $e_n = 0.9, e_t = 0.9$ ($*$); $e_n = 0.8, e_t = 0.8$ ($\times$). The filled symbols and the symbols with superscribed circles show the results obtained using (3.34), while the open symbols and the symbols without superscribed circles show the result using a Gaussian distribution for the relative velocity distribution (3.58). The pair distribution function calculated using the correction proposed by Garzo & Dufty (1999) is indistinguishable from that calculated using (3.58).

The rate of dissipation of energy can be obtained quite easily because the dissipation is only due to the change in the normal velocity at contact

$$D = -\frac{\rho^2 \chi}{2} \int \mathrm{d}\boldsymbol{w} \int \mathrm{d}\boldsymbol{\varpi} \int \mathrm{d}\boldsymbol{k} f(\boldsymbol{w}, \boldsymbol{\varpi}, \boldsymbol{k}) w_n \left(\frac{w_n'^2 - w_n^2}{4} \right), \tag{3.59}$$

where $w_n' = -e_n w_n$ is the post-collisional relative velocity in a collision in which the pre-collisional relative velocity is w_n. Note that in (3.59), we have included the energy dissipation of only one of the particles involved in the collision, and so we do not have the factor (1/2) which takes into account double-counting. The integrals over the tangential component of the relative velocity $\boldsymbol{w}_t$ can be explicitly carried out, to provide

$$D = \frac{\rho^2 \pi \chi (1 - e_n^2)}{2} \int_0^\infty \mathrm{d}w_n f_{wn}^{(0)}(w_n) w_n^3. \tag{3.60}$$

The collision frequency can be written, in terms of the relative velocity distribution, as

$$\begin{aligned} \nu &= \frac{\rho^2 \chi}{2} \int \mathrm{d}\boldsymbol{w} \int \mathrm{d}\boldsymbol{\varpi} \int \mathrm{d}\boldsymbol{k} f(\boldsymbol{w}, \boldsymbol{\varpi}, \boldsymbol{k}) w_n \\ &= 2\pi \rho^2 \chi \int_0^\infty \mathrm{d}w_n f_{wn}^{(0)}(w_n) w_n. \end{aligned} \tag{3.61}$$

The ratio of the rate of dissipation of energy and the collision frequency is

$$\frac{D}{\nu} = \frac{1 - e_n^2}{4} \frac{\displaystyle\int_0^\infty \mathrm{d}w_n f_{wn}^{(0)}(w_n) w_n^3}{\displaystyle\int_0^\infty \mathrm{d}w_n f_{wn}^{(0)}(w_n) w_n}. \tag{3.62}$$

The rate of dissipation of energy for rough particles is little more difficult to calculate, since it is necessary to express the linear and angular velocities of the particles in terms of $\boldsymbol{w}$ and $\boldsymbol{\varpi}$ using (3.11), and then simplify the resulting expressions. After some algebra, we obtain

$$\begin{aligned} D = \frac{-\rho^2 \chi}{2} &\int \mathrm{d}\boldsymbol{w} \int \mathrm{d}\boldsymbol{\varpi} \int \mathrm{d}\boldsymbol{k} f(\boldsymbol{w}, \boldsymbol{\varpi}, \boldsymbol{k}) (\boldsymbol{w}.\boldsymbol{k}) \\ &\times \left(\frac{\mathscr{I}(1 - e_t^2)}{1 + 4\mathscr{I}} (4 w_i (\delta_{ij} - k_i k_j) w_j + \boldsymbol{\varpi}_i (\delta_{ij} - k_i k_j) \boldsymbol{\varpi}_j) \right. \\ &\left. + \frac{4\mathscr{I}(1 + e_t)^2 (1 - 4\mathscr{I})}{(1 + 4\mathscr{I})^2} \epsilon_{ijk} w_i k_j \boldsymbol{\varpi}_k + (1 - e_n^2)(k_i w_i)^2 \right). \end{aligned} \tag{3.63}$$

A direct simplification of the above equation can be used to isolate the contributions to the rate of dissipation due to the tangential and normal impulses,

$$\begin{aligned} D = \frac{\rho^2 \pi \chi (1 - e_n^2)}{2} &\int d w_n f_{w_n}^{(0)} w_n^3 \\ &+ \frac{\rho^2 \chi}{2} \int \mathrm{d}\boldsymbol{w} \int \mathrm{d}\boldsymbol{\varpi} \int \mathrm{d}\boldsymbol{k} f(\boldsymbol{w}, \boldsymbol{\varpi}, \boldsymbol{k}) w_n \left(\frac{\mathscr{I}(1 - e_t^2)}{1 + 4\mathscr{I}} (4 \mathbf{w}_t^2 + \boldsymbol{\varpi}_t^2) \right. \\ &\left. + \frac{4\mathscr{I}(1 + e_t)^2 (1 - 4\mathscr{I})}{(1 + 4\mathscr{I})^2} \epsilon_{ijk} \boldsymbol{w}_{ti} k_j \boldsymbol{\varpi}_{tk} \right). \end{aligned} \tag{3.64}$$

For perfectly smooth particles with $e_t = -1$, it is clear that the rate of dissipation depends only on the distribution function for the normal velocity. In the case of perfectly rough particles, where $e_t = 1$, we find that the rate of dissipation of energy depends only on the distribution $f_{wn}^{(0)}$ because the average of $\epsilon_{ijk} \boldsymbol{w}_{ti} k_j \boldsymbol{\varpi}_{tk}$ is identically zero. In this case, the rate of dissipation of energy reduces to (3.60), which is the same

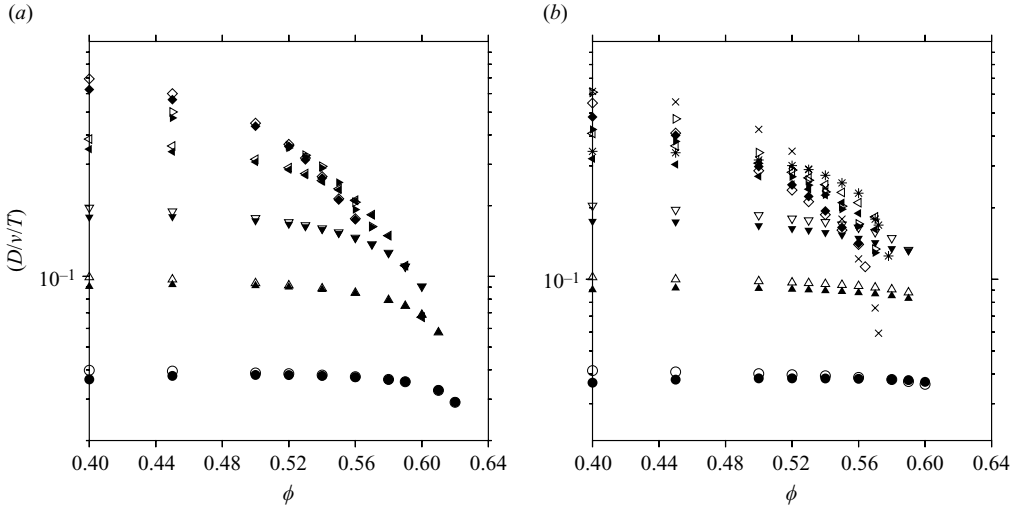

FIGURE 15. The rate of dissipation of energy due to inelastic collisions D, divided by the collision frequency and T, as a function of the volume fraction for smooth particles $e_t = -1$ (a) and for rough particles $e_t = 1$ and $e_t = e_n$ (b), for different normal coefficients of restitution, ($\circ$) $e_n = 0.98$; ($\triangle$) $e_n = 0.95$; (∇) $e_n = 0.9$; ($\triangleleft$) $e_n = 0.8$; ($\triangleright$) $e_n = 0.7$; ($\diamond$) $e_n = 0.6$; ($*$) $e_n = 0.9$, $e_t = 0.9$; ($\times$) $e_n = 0.8$, $e_t = 0.8$. The filled symbols show the results from simulations, while the open symbols show the prediction (3.62) with the relative velocity distribution given by (3.40) for particles with $e_t = 1$ and $e_t = -1$. Only the simulation results are shown for particles with $e_t = e_n$.

as that for smooth particles. In the case of rough particles with $e_t = e_n$, the dissipation rate requires the distribution of linear and angular velocities tangential to the surfaces at contact. This could be done using a Gaussian form as shown in figures 10 and 11, but we do not proceed further as this would involve additional fitting functions.

The ratio of the dissipation rate and the collision frequency, using approximation (3.40) for the normal velocity distribution, with α given by (3.45) and (3.46), and the constant C given by (3.43) and (3.44), is shown in figure 15. It is observed that there is an excellent numerical agreement between predictions of approximate form (3.40) and the actual value obtained in simulations indicating that the dissipation rate can be accurately predicted using a good model for the relative velocity distribution in the dense limit. It is observed that the ratio of the dissipation rate and frequency shows a much larger decrease near the close packing limit for $e_t = e_n = 0.8$. This is related to the larger increase in the parameter α in figure 4 for $e_t = e_n = 0.8$, which results in a much smaller ratio of the dissipation rate and frequency. A similar feature will be observed a little later for the ratio of the components of the stress and the collision frequency.

The collisional stress, due to the collisional transport of momentum, can be written using indicial notation as

$$\sigma_{ij} = \frac{\rho^2 \chi}{2} \int \mathrm{d}\boldsymbol{w} \int \mathrm{d}\boldsymbol{\varpi} \int \mathrm{d}\boldsymbol{k}\, f(\boldsymbol{w}, \boldsymbol{\varpi}, \boldsymbol{k}) w_n(\Delta u_i) k_j, \tag{3.65}$$

where Δu_i, the impulse in a collision, is $(\Delta w_i/2)$, where Δw_i is the change in the velocity difference between the two particles. We first examine the case of smooth particles, for which the impulse is along the line joining the centres $\boldsymbol{k}$, and

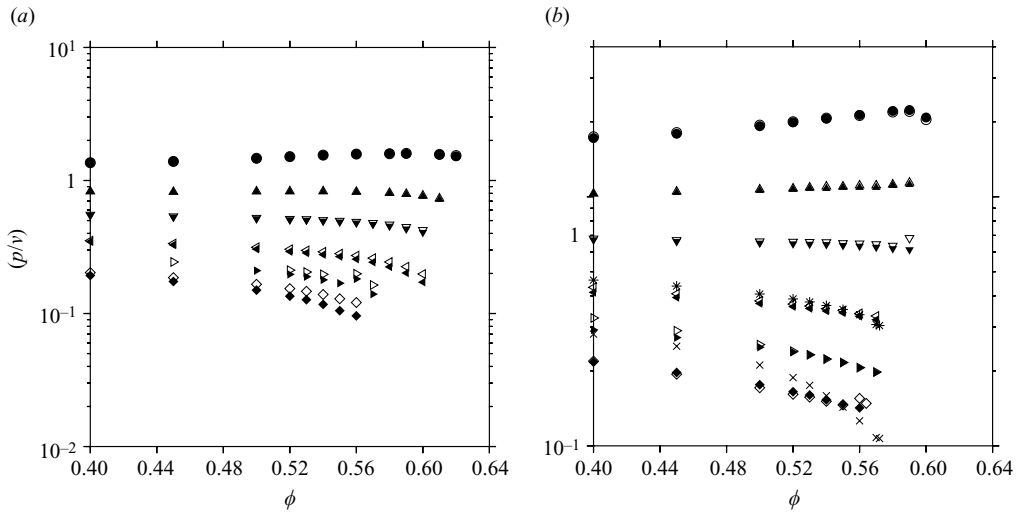

FIGURE 16. The isotropic part of the stress tensor divided by the collision frequency (p/ν), as a function of the volume fraction for smooth particles $e_t = -1$ (a) and for rough particles $e_t = 1$ (b), for different normal coefficients of restitution, $(\bigcirc)$ $e_n = 0.98$; $(\triangle)$ $e_n = 0.95$; (∇) $e_n = 0.9$; $(\triangleleft)$ $e_n = 0.8$; $(\triangleright)$ $e_n = 0.7$; $(\diamond)$ $e_n = 0.6$; $(*)$ $e_n = 0.9, e_t = 0.9$; $(\times)$ $e_n = 0.8, e_t = 0.8$. The filled symbols show the results from simulations, while the open symbols show the prediction (3.68) with the relative velocity distribution given by (3.40) for particles with $e_t = 1$ and $e_t = -1$. Only the simulation results are shown for particles with $e_t = e_n$.

$\Delta w_i = -(1 + e_n) w_n k_i$. In this case, the stress is given by

$$\sigma_{ij} = \frac{\rho^2 \chi (1 + e_n)}{4} \int \mathrm{d}\boldsymbol{w} \int \mathrm{d}\boldsymbol{k} f(\boldsymbol{w}, \boldsymbol{k}) w_n^2 k_i k_j. \tag{3.66}$$

The pressure $p = (\sigma_{ii}/3)$ is only due to the normal component of the impulse on the particles

$$p = \frac{\pi \rho^2 \chi (1 + e_n)}{3} \int \mathrm{d}w_n \, w_n^2 f_{wn}^{(0)}(w_n). \tag{3.67}$$

The ratio of the pressure and the collision frequency is given by

$$\frac{p}{\nu} = \frac{(1 + e_n)}{6} \frac{\int \mathrm{d}w_n \, w_n^2 f_{wn}^{(0)}(w_n)}{\int \mathrm{d}w_n \, w_n f_{wn}^{(0)}(w_n)}. \tag{3.68}$$

The ratio of the pressure and the collision frequency, using approximation (3.40) for the normal velocity distribution, with the constants α given by (3.45) and (3.46) and C given by (3.43) and (3.44), is shown in figure 16. It is observed that there is excellent numerical agreement between approximate form (3.40) and the actual value obtained for rough particles. This is because, as can be seen from figure 2, the exponential approximation for the distribution function is a very good approximation for rough particles. The agreement for smooth particles is also numerically very good over the range of coefficients of restitution examined here, though it is not as good as that for rough particles. This is because of the deviation of the actual distribution function from the exponential distribution, as shown in figure 1. Therefore, it is clear that

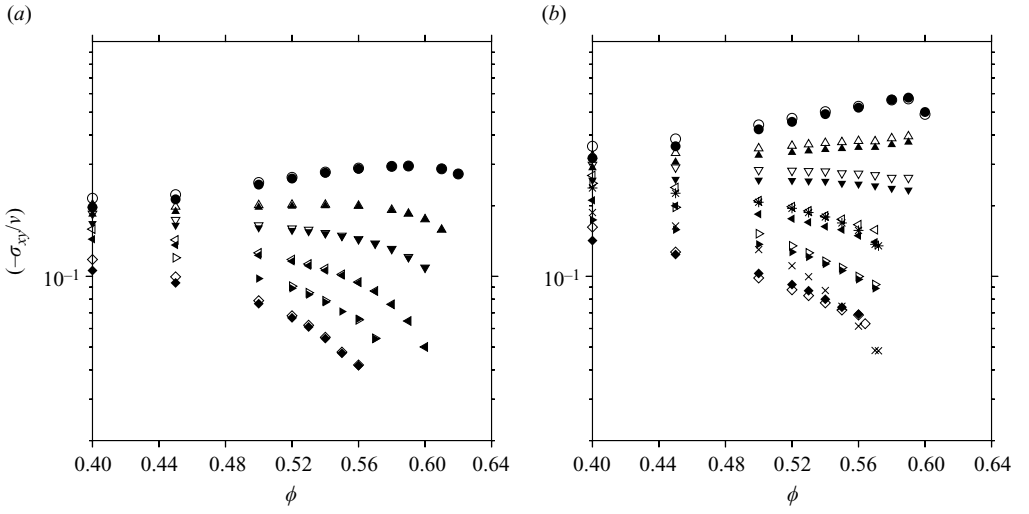

FIGURE 17. The negative of the shear stress divided by the collision frequency $(-\sigma_{xy}/\nu)$, as a function of the volume fraction for smooth particles ($e_t = -1$) (*a*) and for rough particles ($e_t = 1$) (*b*), for ($\bigcirc$) $e_n = 0.98$; ($\triangle$) $e_n = 0.95$; (∇) $e_n = 0.9$; ($\triangleleft$) $e_n = 0.8$; ($\triangleright$) $e_n = 0.7$; ($\diamond$) $e_n = 0.6$; (*) $e_n = 0.9$, $e_t = 0.9$; ($\times$) $e_n = 0.8$, $e_t = 0.8$. The filled symbols show the results from simulations, while the open symbols show the prediction obtained from the dissipation rate (3.62) using the energy balance equation, with the relative velocity distribution given by (3.40) for particles with $e_t = 1$ and $e_t = -1$. Only the simulation results are shown for particles with $e_t = e_n$.

the pressure can be accurately predicted using a good model for the relative velocity distribution in the dense limit.

The shear stress can be obtained from the velocity distribution function in two ways. The first is to use the energy balance condition to obtain the shear stress from the rate of dissipation of energy. The stress obtained in this manner, shown in figure 17, is in excellent agreement with the simulation results for both rough and smooth particles; this is not surprising because the stress has been obtained from the dissipation rate, and (3.40) was found to predict the dissipation rate very well. The other approach is to use the decomposition of the normal velocity distribution in spherical harmonics in order to obtain the shear stress. For smooth particles, there is no tangential impulse at the point of collision. Therefore, the integral over the tangential velocity can be explicitly carried out to obtain the shear stress. However, for rough particles, the tangential impulse has to be incorporated, and the stress calculated using only the normal impulse will provide only a part of the total shear stress. In order to distinguish between the two contributions, we define the shear stress due to the normal impulse as

$$\sigma_{xy}^{n} = \rho^2 \chi \int \mathrm{d}\boldsymbol{w} \int \mathrm{d}\boldsymbol{\varpi} \int \mathrm{d}\boldsymbol{k}\, f(\boldsymbol{w}, \boldsymbol{\varpi}, \boldsymbol{k}) w_n((\Delta u_i)k_i)k_x k_y, \tag{3.69}$$

where $(\Delta u_i)k_i$ is the component of the impulse along the line joining the centres of the particles. The expression for the shear stress due to the normal impulse can be simplified using $\Delta u_i = -((1 + e_n)w_i/2)$, and integrating over the angular velocity distribution and the tangential component of the linear velocity distribution, to obtain

$$\sigma_{xy}^{n} = 2\pi\rho^2\chi(1 + e_n)\sqrt{\frac{\pi}{15}} \int_0^\infty \mathrm{d}w_n\, w_n^2 f_{wn}^{(1)}(w_n). \tag{3.70}$$

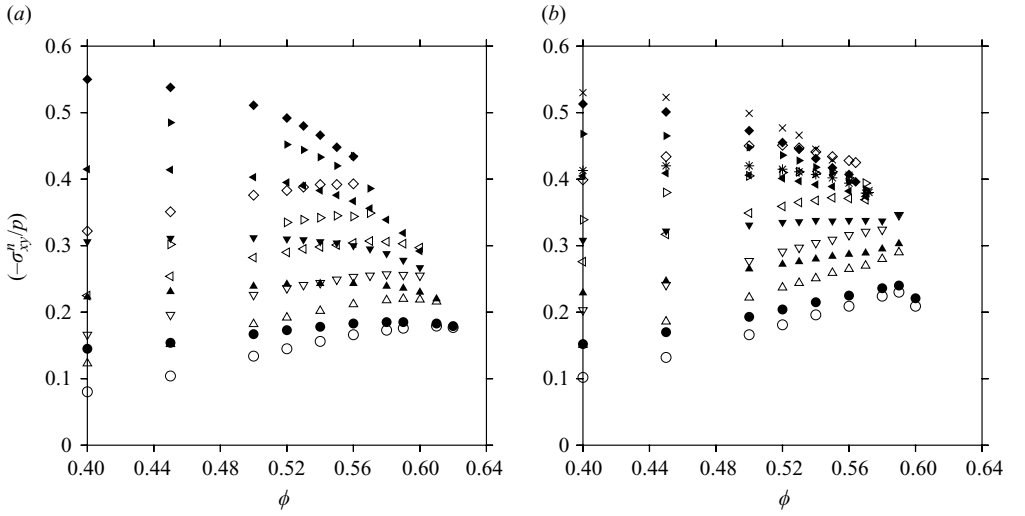

FIGURE 18. The negative of the shear stress due to normal impulse divided by the pressure $(-\sigma^n_{xy}/p)$, as a function of the volume fraction for, (*a*) smooth particles ($e_t = -1$) and (*b*) rough particles ($e_t = 1$), for (○) $e_n = 0.98$; (△) $e_n = 0.95$; (▽) $e_n = 0.9$; (◁) $e_n = 0.8$; (▷) $e_n = 0.7$; (◇) $e_n = 0.6$; (*) $e_n = 0.9, e_t = 0.9$; (×) $e_n = 0.8, e_t = 0.8$. The filled symbols show the results from simulations, while the open symbols show the prediction of (3.72) for particles with $e_t = 1$ and $e_t = -1$. Only the simulation results are shown for particles with $e_t = e_n$.

The ratio of σ^n_{xy} and the pressure is given by

$$\frac{\sigma^n_{xy}}{p} = 6\sqrt{\frac{\pi}{15}}\frac{\displaystyle\int_0^\infty \mathrm{d}w_n\, w_n^2 f^{(1)}_{wn}}{\displaystyle\int_0^\infty \mathrm{d}w_n\, w_n^2 f^{(0)}_{wn}}. \tag{3.71}$$

The above relationship is exact, and we have verified that the simulation results are in numerical agreement to within 0.1 %. An approximation can be made if we assume that the ratio of the distribution functions $f^{(1)}_{wn}$ and $f^{(0)}_{wn}$ is independent of velocity. In this case, the ratio of the shear stress and the pressure can be written as

$$\frac{\sigma^n_{xy}}{p} = 6\sqrt{\frac{\pi}{15}}c^{(1)}_{wn}, \tag{3.72}$$

where $c^{(1)}_{wn}$ is defined in (3.57).

The ratio $(-\sigma^n_{xy}/p)$ is shown as a function of volume fraction for different coefficients of restitution in figure 18. Here, the purpose is to test the approximation that $(f^{(1)}_{wn}/f^{(0)}_{wn})$, $(f^{(2)}_{wn}/f^{(0)}_{wn})$ and $(f^{(3)}_{wn}/f^{(0)}_{wn})$ are independent of the relative velocity w_n. The filled symbols are the simulation results, while the open symbols show the result obtained using approximation (3.72). It is observed that there is fairly good quantitative agreement for the normal component of the shear stress for rough particles in the range $0.52 \leqslant \phi \leqslant \phi_{max}$. This indicates that approximation (3.72), which assumes that the ratio $(f^{(1)}_{wn}/f^{(0)}_{wn})$ is independent of w_n is a good one for rough particles. The agreement is not as good for smooth particles, and there are errors of the order of 15 % in the dense limit.

Since the stress due to the normal impulse provides only a part of the shear stress for rough particles, it is of interest to determine the ratio of the shear stress due to

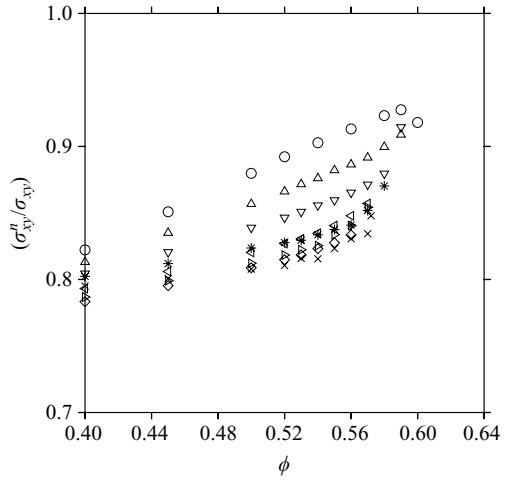

FIGURE 19. The ratio of the shear stress due to the normal impulse between particles σ^n_{xy} and the total shear stress σ_{xy} as a function of volume fraction ϕ for rough particles, ($\bigcirc$) $e_n = 0.98$, $e_t = 1.0$; ($\triangle$) $e_n = 0.95$, $e_t = 1.0$; (∇) $e_n = 0.9$, $e_t = 1.0$; ($\triangleleft$) $e_n = 0.8$, $e_t = 1.0$; ($\triangleright$) $e_n = 0.7$, $e_t = 1.0$; ($\diamond$) $e_n = 0.6$, $e_t = 1.0$; ($*$) $e_n = 0.9$, $e_t = 0.9$; ($\times$) $e_n = 0.8$, $e_t = 0.8$.

normal impulse and the total shear stress. This ratio is shown in figure 19, where it is observed that $(\sigma^n_{xy}/\sigma_{xy})$ varies in a narrow range between about 0.8 and 0.9 for the entire range of volume fractions and coefficients of restitution considered here. For rough particles with coefficient of restitution in the range 0.6–0.7, the ratio is very close to 0.8, and is nearly independent of volume fraction for $\phi > 0.52$. This implies that the stress due to the tangential impulse at contact is not more than 10–20 % of the total stress even in rough particles with coefficient of restitution $e_t = 1$, and the shear stress can be well approximated as the stress due to the normal impulse even for rough particles. This is significant, because the stress due to the normal impulse can be calculated from the normal velocity distribution alone, and it is not necessary to have a model for the distribution of the relative velocity tangential to the surfaces of contact.

The normal stress differences can be determined from the distributions $f^{(2)}_{wn}$ and $f^{(3)}_{wn}$ in a manner similar to (3.72) for the shear stress. It can easily be shown, based on symmetry arguments, that the components σ_{xx}, σ_{yy} and σ_{zz} result only from the normal impulse between particles at contact; there is no contribution to these components due to the tangential impulse at contact in a simple shear flow. Using this simplification, the final results for the ratio of the normal stress differences and the pressure are

$$\frac{\sigma_{xx} - \sigma_{yy}}{p} = 12\sqrt{\frac{\pi}{15}}\frac{\displaystyle\int_0^\infty \mathrm{d}w_n\, w_n^2 f^{(3)}_{wn}}{\displaystyle\int_0^\infty \mathrm{d}w_n w_n^2 f^{(0)}_{wn}} \tag{3.73}$$

$$\frac{\sigma_{yy} - \sigma_{zz}}{p} = -6\sqrt{\frac{\pi}{15}}\frac{\displaystyle\int_0^\infty \mathrm{d}w_n\, w_n^2 f^{(3)}_{wn}}{\displaystyle\int_0^\infty \mathrm{d}w_n w_n^2 f^{(0)}_{wn}} - 6\sqrt{\frac{\pi}{5}}\frac{\displaystyle\int_0^\infty \mathrm{d}w_n\, w_n^2 f^{(2)}_{wn}}{\displaystyle\int_0^\infty \mathrm{d}w_n w_n^2 f^{(0)}_{wn}}. \tag{3.74}$$

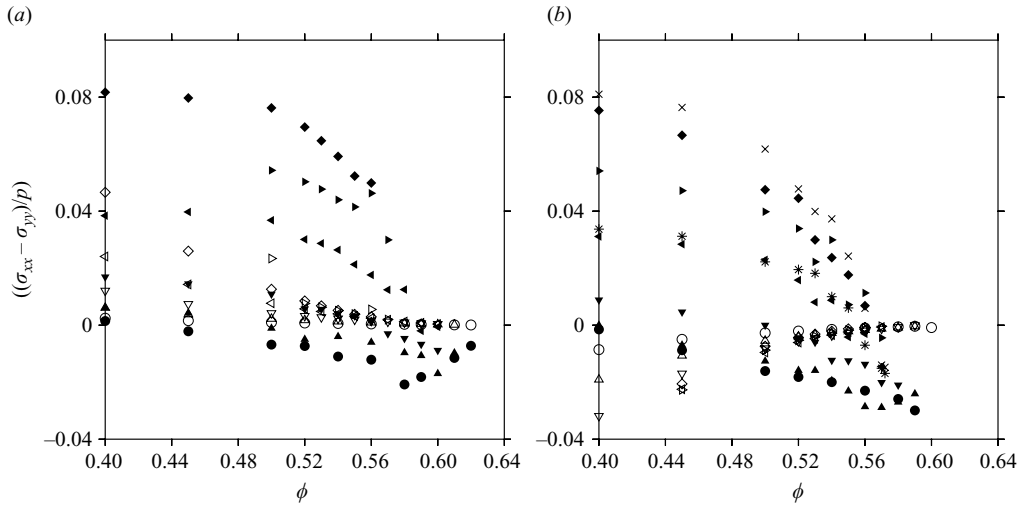

FIGURE 20. The scaled first normal stress difference $((\sigma_{xx}-\sigma_{yy})/p)$, as a function of the volume fraction for smooth particles $e_t=-1$ (a) and for rough particles $e_t=1$ (b), for different normal coefficients of restitution, ($\bigcirc$) $e_n=0.98$; ($\triangle$) $e_n=0.95$; (∇) $e_n=0.9$; ($\triangleleft$) $e_n=0.8, e_t=1.0$; ($\triangleright$) $e_n=0.7, e_t=1.0$; ($\diamond$) $e_n=0.6, e_t=1.0$; (*) $e_n=0.9, e_t=0.9$; ($\times$) $e_n=0.8, e_t=0.8$. The filled symbols show the results from simulations, while the open symbols show the results of (3.75) for particles with $e_t=1$ and $e_t=-1$. Only the simulation results are shown for particles with $e_t=e_n$.

If we assume that the ratios $(f_{wn}^{(2)}/f_{wn}^{(0)})$ and $(f_{wn}^{(3)}/f_{wn}^{(0)})$ are independent of velocity w_n, then (3.73) and (3.74) can be simplified

$$\frac{\sigma_{xx}-\sigma_{yy}}{p}=12\sqrt{\frac{\pi}{15}}c_{wn}^{(3)} \tag{3.75}$$

$$\frac{\sigma_{yy}-\sigma_{zz}}{p}=-6\sqrt{\frac{\pi}{15}}c_{wn}^{(3)}-6\sqrt{\frac{\pi}{5}}c_{wn}^{(2)}. \tag{3.76}$$

The results of the above approximation, with $c_{wn}^{(2)}$ and $c_{wn}^{(3)}$ given by (3.57), are shown in figures 20 and 21.

The simulation results show that the magnitude of the first normal stress difference is significantly smaller than the second normal stress difference. In addition, the first normal stress difference could be either positive or negative, while the second normal stress difference is always positive. Both of these observations are in agreement with the results based on the Enskog approximation (Kumaran 2006*a*), as well as with simulation results (Silbert *et al.* 2001). For the second normal stress difference depicted in figure 21, the agreement between the theoretical predictions and the simulation results is quite good for coefficient of restitution 0.9 and above. The agreement is poorer as the coefficient of restitution decreases, primarily because the approximation that the distribution ratio is a constant, implicit in (3.57), becomes poorer as collisions become more inelastic. If we use the actual distributions calculated in the simulations in (3.74) for calculating the normal stress differences, we obtain results accurate to within 1 % of the value obtained in simulations. The qualitative trends of the second normal stress difference are well captured by the theory. The agreement is poorer for the first normal stress difference for smooth particles. This is because the first normal stress difference involves calculating the small difference of two stress components

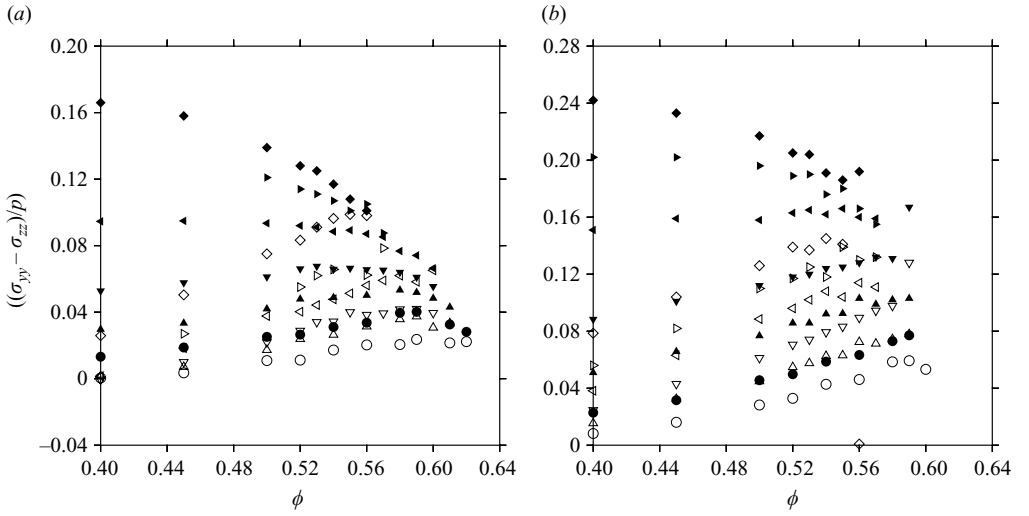

FIGURE 21. The scaled second normal stress difference $((\sigma_{yy}-\sigma_{zz})/p)$, as a function of the volume fraction for smooth particles $e_t=-1$ (*a*) and for rough particles $e_t=1$ (*b*), for different normal coefficients of restitution, ($\circ$) $e_n=0.98$; ($\triangle$) $e_n=0.95$; (∇) $e_n=0.9$; ($\triangleleft$) $e_n=0.8$, $e_t=1.0$, ($\triangleright$) $e_n=0.7$, $e_t=1.0$; ($\diamond$) $e_n=0.6$, $e_t=1.0$; ($*$) $e_n=0.9$, $e_t=0.9$; ($\times$) $e_n=0.8$, $e_t=0.8$. The filled symbols show the results from simulations, while the open symbols show the results of (3.76) for particles with $e_t=1$ and $e_t=-1$. Only the simulation results are shown for particles with $e_t=e_n$.

σ_{xx} and σ_{yy} which are nearly equal in value, and the numerical errors are quite large.

As an application of the model developed here to a system of practical interest, we consider the relation between the volume fraction and the angle of inclination for the flow down an inclined plane, which is inclined at an angle θ to the horizontal. The flow down an inclined plane has several striking features whose physical mechanisms are just beginning to be understood. Even though the flow is relatively dense, with volume fraction between 52 % and 58 %, recent work (Reddy & Kumaran 2007) indicates that particle interactions are dominated by binary contacts for particles with shear modulus comparable to sand or glass. Even for softer particles where there are multiple contacts, it has been found that brief binary contacts dominate (Silbert *et al.* 2007). Many of the qualitative features of the flow have been understood on the basis of constitutive relations derived using the Enskog procedure (Kumaran 2008), where the transmission of stress is assumed to be due to binary collisions. Though the earlier analysis of Kumaran (2006*a*, 2008) did explain all the qualitative features of the inclined plane flow, the quantitative estimates for the angle of repose, and the variation of the angle of inclination with volume fraction, were not in agreement with simulations. It was suggested that the poor agreement may be because the relative velocity distributions were affected by the correlations between particles. Since we have calculated the relative velocity distributions in a dense flow in the present analysis, we re-calculate the angle of repose and the variation of the volume fraction with angle of inclination using the model proposed here.

From momentum balance, the rate of change of the shear and normal stresses perpendicular to the plane of the flow are equal to the body forces in the respective

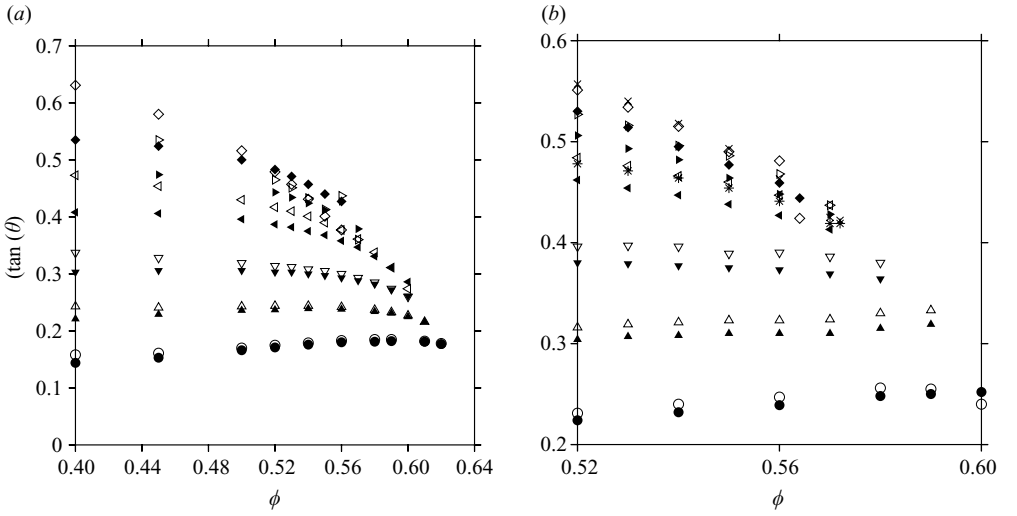

FIGURE 22. The tangent of the angle of inclination, $\tan(\theta) = -(\sigma_{xy}/\sigma_{yy})$, as a function of the volume fraction for smooth particles with $e_t = -1.0$ (a) and rough particles with $e_t = 1.0$ (b) and for ($\bigcirc$) $e_n = 0.98$; ($\triangle$) $e_n = 0.95$; (∇) $e_n = 0.9$; ($\triangleleft$) $e_n = 0.8, e_t = 1.0$; ($\triangleright$) $e_n = 0.7, e_t = 1.0$; ($\diamond$) $e_n = 0.6, e_t = 1.0$; ($*$) $e_n = 0.9, e_t = 0.9$; ($\times$) $e_n = 0.8, e_t = 0.8$. The solid symbols show the results of the simulations, and the open symbols show the results of the model using (3.40) for the relative velocity distribution, with α given by (3.45) and (3.46), C given by (3.43) and (3.44), the pressure given by (3.68) (we assume $\sigma_{yy} = p$ in the model), the shear stress obtained as the ratio of dissipation rate and strain rate, and the dissipation rate obtained from (3.62) for particles with $e_t = 1$ and $e_t = -1$. Only the simulation results are shown for particles with $e_t = e_n$.

directions

$$(\mathrm{d}\sigma_{xy}/\ \mathrm{d}y) = -\rho g \sin(\theta),$$
$$(\mathrm{d}\sigma_{yy}/\mathrm{d}y) = \rho g \cos(\theta). \tag{3.77}$$

The ratio of the shear and normal stresses is a constant in the flow

$$(\sigma_{xy}/\sigma_{yy}) = -\tan(\theta). \tag{3.78}$$

The above ratio can be used to determine the variation of $\tan(\theta)$ with volume fraction for smooth and rough particles with different coefficients of restitution. The simulation results are compared with the theoretical model predictions using (3.68) for the pressure, and (3.62) for the dissipation rate, and using the energy balance condition that the dissipation rate is the product of the shear stress and strain rate in figure 22. The filled symbols show the results from simulations, while the open symbols are the prediction of the model. It is observed that the difference between the simulation results and the model prediction is equivalent to a difference in angle of only about 1°.

4. Conclusions

At the outset, it is important to note that the simulations carried out here have all been on relatively small systems of 500 particles. In addition, the event-driven simulations were able to access a maximum volume fraction in the range 0.56 (for $e_n = 0.6$) to 0.62 (for $e_n = 0.98$), and so results for higher volume fractions were

obtained by extrapolation. It is necessary to carry out simulations of larger sizes, and it is possible that the numerical values of the results obtained here will change slightly if larger system sizes are used, and simulations of higher numerical accuracy are used to probe higher volume fractions. However, the simulation studies have given us fundamental insights into several aspects of the shear flow of inelastic particles, and have clarified a number of puzzles that have existed previously in literature. The nature of the insights obtained are likely to be more robust, and to hold even for larger systems. We discuss these in detail, and place them in the context of previous studies.

4.1. *Ordering*

One of the important results is the lack of icosahedral or planar ordering in sheared systems, provided the system size is sufficiently large. In an equilibrium elastic fluid, there is a crystallization transition at a volume fraction of 0.49, as evidenced by the increase in the icosahedral order parameter Q_6 from zero to a value slightly higher than 0.5. In a sheared fluid of inelastic particles, we find that there is no transition to an ordered structure if the system size is sufficiently large, and the system continues to be in a random state with Q_6 near zero. However, when the system size is small, there appears to be first an ordering transition, and then subsequent disordering when the volume fraction is further increased. It appears that the ordered state is unstable to perturbations with wavelength greater than a minimum value, and undergoes a spontaneous transition to the random state; this transition requires further systematic study.

There is a significant difference in the structure between the equilibrium and sheared states, so that the order parameter and the pair distribution function in the sheared state cannot be expressed simply as a small perturbation about their values in the equilibrium state. Another method that has been proposed (Lutsko 1996) is an expansion of the pair distribution function for the shear flow in powers of the strain rate, in which the leading contribution is the equilibrium distribution function. This expansion is also not likely to accurately represent dense sheared flows, since the structure in the equilibrium and sheared states are so different.

It should be noted that this transition is different from the shear melting transition in colloidal crystals (Stevens & Robbins 1993; Lahiri & Ramaswamy 1994) for particles which have long-range electrostatic interactions. In a colloidal crystal, the melting of a solid to a liquid is induced by an increase in the strain rate at constant temperature, and the temperature and strain rate are independent variables. Since there is an energy scale which characterizes the strength of the interaction between particles, the temperature is usually scaled by the interaction potential between particles, while the shear rate is scaled by the diffusion time. A similar distinction can also be drawn with the ordering in a sheared elastic or thermostatted fluid (Kirkpatrick & Nieuwoudt 1986; Lutsko & Dufty 1986; Lutsko 1996), where the temperature and the strain rate can be varied independently, and where shear ordering can be obtained as the strain is increased. Here, a non-dimensional strain rate can be defined by scaling the strain rate by the square root of the temperature of the system. In the present case, there is a coupling between the temperature and the strain rate due to energy balance, and so the strain rate can be set equal to 1 without loss of generality. Consequently, the state of order of the system depends only on the volume fraction of the particles and the system size.

The ordering in the present system is also different from the shear ordering in low-Reynolds-number suspensions (Foss & Brady 2000), where the ordering is induced

by changes in the Péclet number. The strain rate in suspensions is also scaled by the inverse of the diffusion time, and the ratio is the square root of the Péclet number. In the present system, the strain rate and the temperature are coupled through the energy balance equation, and since all time scales can be scaled by the inverse of the strain rate, the transition cannot be induced by variation in the strain rate. The only relevant parameters for the order–disorder transition (apart from the wavelength or box size) are the volume fraction and the coefficients of restitution. Therefore, shear ordering and disordering in the present system is qualitatively different from that observed in systems such as colloidal crystals or suspensions in previous studies. It should also be noted that the aforementioned studies were carried out at lower volume fractions than that in the present analysis, where we have specifically examined the approach to the close packing limit. It is likely that the results obtained for moderately dense systems may not be applicable as the close packing limit is approached.

This indicates that previous simulation results indicating the presence of ordering in sheared systems (Kumar & Kumaran 2006) should be treated with care, because the validity of these results is limited to small simulation cells; it is likely that the ordering would have disappeared if the simulation cells were made larger. The present analysis indicates that the rheology of a granular shear flow is coupled to the ordering, and it underscores the importance of monitoring the order parameters when rheological experiments or simulations are performed. This is of particular importance when comparing the rheology in different flow systems (GDR MiDi 2004; Delannay *et al.* 2007), since the order parameter may vary from system to system, and it may also vary within a system between the bulk flow and the flow near boundaries.

The presence of ordering in small systems also has implications for the flow near boundaries, since the presence of a flat surface bounding a flow of monodisperse particles is likely to order the particles near the boundary. Simulations consistently show a signature of ordering, which is the layering of particles, at boundaries (see, for example, Delannay *et al.* 2007). However, the planar and icosahedral order parameters are seldom probed near the boundaries. Since the rheology of the system is dependent on the state of ordering in the system, it is essential to incorporate this in theories when treating the flow near boundaries. This could explain why theories based on the assumption of a random state typically predict a small increase in the volume fraction at the boundaries, but this increase is seldom observed in simulations.

Finally, we should note that ordering is a phenomenon largely restricted to monodisperse spherical particles. A small amount of polydispersity is likely to destroy order (in addition to generating other complications like segregation), and so the random state is definitely more applicable to real systems. The ordered state is very limited in its applicability, and the ordering near boundaries for the flow of monodisperse particles is not likely to be observed in real systems with a small amount of polydispersity. Therefore, it is more natural to consider the random state in the context of practical applications.

4.2. *Collision frequency and pair distribution function*

An important result of the present analysis is that the collision frequency in a sheared granular flow diverges at a lower volume fraction than $\phi_c = 0.64$ for random close packing. The volume fraction at which the collision frequency diverges is designated as ϕ_{ad}, the volume fraction for arrested dynamics, where the collision frequency and stress go to infinity at constant strain rate, or the strain rate goes to zero at constant stress. The equivalent volume fraction for an elastic hard-particle system in the absence of shear is the random close packing volume fraction $\phi_c = 0.64$, where the

collision frequency diverges at constant temperature. The term 'arrested dynamics' is used here to distinguish it from the other volume fractions such as the jamming, isostatic and close-packing.

It is clear that the arrest of particle motion under shear, as the volume fraction is increased, is a dynamical phenomenon; the analogue in an equilibrium hard sphere system is the random close packing volume fraction where the collision frequency diverges at constant temperature. Another important finding regarding the volume fraction for arrested dynamics is that the variance of the relative velocity distribution of pairs of particles along the line joining their centres seems to show a decrease to zero as the volume fraction is approached, though the rate of decrease is weak (logarithmic for rough particles). This indicates that the degrees of freedom corresponding to the relative motion between pairs of particles is getting arrested faster than that for single particle motion.

The functional form of the variation of the collision frequency with volume fraction also depends on the coefficient of restitution. For rough particles, it is found that the volume ϕ_{ad} at which the frequency diverges decreases from 0.64 for elastic particles to a minimum of about 0.58 as the coefficient of restitution is decreased. In addition, whereas the collision frequency increases proportionally to $(\phi_c - \phi)^{-1}$ near the random close packing volume fraction, it shows a power law increase proportional to $(\phi_{ad} - \phi)^a$ near the volume fraction for arrested dynamics, where the exponent a increases from 1 as the particles are made more inelastic.

It is important to note that for particles with elastic interactions, the volume fraction of 0.64 is of significance only for hard monodisperse spheres. If particles can be deformed without breaking, then it would be possible to achieve volume fractions close to 1.0. However, the volume fraction of 0.64 still has significance, in that it is the maximum volume fraction that can be achieved for hard particles. In the context of soft particles, the implication is that the system has to transition to a multi-body contact regime at or lower than the volume fraction lower than 0.64; the transition volume fraction will approach 0.64 as the particle stiffness is increased. In the present analysis, we have found that the arrested dynamics volume fraction (defined as the volume fraction at which the collision frequency diverges) is lower for a sheared inelastic fluid of hard particles; this implies that in soft-particle systems under shear, the transition from a binary contact regime to a multi-body contact regime should take place at a lower volume fraction than that for elastic particles in the absence of shear. This enables us to resolve some apparent inconsistencies in previous soft-particle simulation results.

One of the puzzling features observed in simulations of dense granular flows down an inclined plane (Silbert *et al.* 2001), is that the maximum volume fraction at the initiation of flow seems to be about 59 %, whereas the maximum volume fraction attainable for random close packing of elastic particles is 64 %. The present analysis indicates that the maximum close packing volume for a shear flow depends on the coefficient of restitution, and the numerical figure of 58.5 % for the lowest coefficients of restitution is close to the value of 59 % observed in simulations of flow down an inclined plane. The discrepancy of less than 1 % between the two values could be because the system sizes used here are too small. It is also possible that for the volume fraction between 58 % and 59 %, the flow is no longer in the binary contact regime, and it is necessary to incorporate multiple contacts in order to accurately capture the rheology of the flow.

The present simulations may not be able to capture the angle of repose if the system is in the multi-body contact regime just before the flow stops. However, the

multi-body contact regime is often associated with chains of particles which transmit stress from one boundary to the other. This requires a compressive load at both boundaries. The flow down an inclined plane does not have a compressive load at the free surface, and so it is difficult to see how stress could be transmitted by force chains. That is the reason why the maximum volume fraction in inclined plane flows is about 59 %, which is the volume fraction at which there should be a transition from a binary contact regime to a multi-body contact regime for very stiff particles.

The pair distribution function is usually derived from the collision frequency using (3.58). The present analysis indicates that this equation is not accurate in dense flows of inelastic particles, because the distribution function for the relative normal velocities of the particles is not a Gaussian distribution. It should be noted that the definition of the pair distribution function we have used here is not the usual thermodynamic definition, but rather a definition which provides the correct frequency of collisions between particles. This is more appropriate for a dense flow, because we are interested in the collisional transport of momentum and energy in order to derive constitutive relations, and it is appropriate to choose the pair distribution function in such a way that it provides the correct collision probability for particles that are approaching each other prior to collision. We find that there is a significant numerical difference between the pair distribution function calculated in this manner, and that derived previously in literature (Mitarai & Nakanishi 2007) using (3.58), or the pair distribution function of Garzo & Dufty (1999) which incorporates the inelasticity of the particles. The pair distribution function also diverges much faster than the Carnahan–Starling pair distribution function, or the high density pair distribution function of Torquato (1995). The magnitude of the deviation from the equilibrium distribution in a shear flow is also much larger than that observed by Luding (2001) for dense hard disc systems in the absence of shear. It should be noted that the analysis of Luding (2001) considers both the random and the ordered branches in two dimensions. In contrast, we do not find an ordered state for a shear flow of inelastic particles when the coefficient of restitution is less than about 0.9. In the study of sheared hard core fluids by Lutsko (2001), the maximum increase in the pair distribution function at volume fractions of about 25 % was found to be about 1 at contact. The present difference in the pair distribution function is much larger; in addition, the present analysis indicates a divergence of the pair distribution function at a lower volume fraction than that for an elastic fluid.

4.3. *Diffusion*

In all the simulation studies carried out it was found that the diffusion coefficient is always non-zero for the random state, but it decreases almost discontinuously to zero when there is an ordering transition. This suggests that previous simulation results, indicating that there is no diffusion in sheared granular materials with volume fraction of above 55 % (Campbell 1997), are valid only if the system size is sufficiently small, so that there is ordering. The trends shown by the diffusion coefficients are qualitatively similar to those in simulations of viscous suspensions of lower volume fraction (Dufty 1984; Foss & Brady 2000); the diffusion coefficient in the flow direction D_{xx} is always larger than those in the gradient (D_{yy}) and vorticity (D_{zz}) directions. The coefficient D_{yy} could be smaller or larger than D_{zz} depending on the volume fraction and coefficient of restitution. The diffusion coefficient D_{xy} is an order of magnitude smaller than the other diffusion coefficients, and it fluctuates between positive and negative values. The standard deviation in the measurement of D_{xy} is comparable to the mean value itself, leading us to conclude that D_{xy} is zero within

the numerical accuracy that can be obtained in simulations. It is found that there is a smaller variation in the diffusion coefficient when it is scaled by the strain rate than the granular temperature.

The diffusive nature of the particle motion was verified by analysing the intermediate scattering function for this flow. If the particles are in diffusive motion, the intermediate scattering function decreases proportionally to $\exp(-D_{ij}k_ik_jt)$, where $\boldsymbol{k}$ is the wavenumber and D_{ij} is the tensor of diffusion coefficients in the different directions. In a dense liquid, in contrast, there are two distinct relaxation processes, the fast β relaxation corresponding to the equilibration of a particle within the cage made up of neighbouring particles, and the slow α relaxation corresponding to cage breakage and escape at long times. There is virtually no decrease in the intermediate scattering function in the β relaxation process because the particle position is fluctuating only within its cage.

For a fluid of elastic particles in the absence of shear, we find that the intermediate scattering functions show almost no decrease with time, because the system has crystallized and the particles are trapped in cages created by the neighbouring particles. The simulations are able to access only the β relaxation process, because the α relaxation process is very slow after crystallization. In contrast, in a sheared inelastic fluid, it is found that the intermediate scattering function decays proportionally to $\exp(-D_{ij}k_ik_jt)$ even at volume fractions as large as 0.57 in the simulations. There are no distinct β and α relaxation processes, and the diffusion process can be described with just one diffusion coefficient. The diffusion coefficients calculated from the intermediate scattering function were in close agreement with those calculated from the mean square displacement.

4.4. *Velocity autocorrelation function*

The velocity autocorrelation function in a dense sheared granular flow was also analysed in the simulations. For an elastic gas at equilibrium, it is well known that the velocity autocorrelation function decays proportionally to $t^{-3/2}$ due to the diffusive nature of momentum transport. This slow decay is referred to as the 'long time tail' in the velocity autocorrelation function. In a dense liquid, on the other hand, particles are confined within cages formed by neighbouring particles, and the correlation time for the velocity is very small because it is the time taken for a particle to rattle within its cage.

Though the structure and diffusion in an inelastic sheared granular flow resembles a system with no caging, we find that the velocity autocorrelation function decreases much faster than the $t^{-3/2}$ scaling for an elastic fluid at equilibrium with no caging effects (Dorfman & Cohen 1972). There was an earlier prediction (Kumaran 2006*c*) that the velocity autocorrelation function should decay as $t^{-9/2}$ in a dense granular flow because energy is not conserved over length scales larger than the conduction length. More recent calculations (Kumaran 2009*a*, *b*) indicate that the scaling laws for the decay of the velocity autocorrelation function are anisotropic, the decay is much faster than the $t^{-3/2}$ scaling law for an elastic fluid at equilibrium. There is also recent experimental evidence (Orpe *et al.* 2008) for the fast decay of the velocity autocorrelation function.

The decay in the velocity autocorrelation function in our simulations is consistent with the above prediction for both rough particles as well. However, scaling laws cannot be definitively verified because the decay is very fast and the time window over which the scaling is observed is not sufficiently long. However, the present simulations do indicate that the decay of the velocity autocorrelation in a dense

granular flow is much faster than the $t^{-3/2}$ decay expected for a normal fluid even for rough particles. This has significant implications for the renormalization of the transport coefficients due to correlations in dense gases (Ernst *et al.* 1978; Kumaran 2006*c*).

4.5. *Granular temperature*

We find that the equipartition approximation is a good one in a dense flow, and the energy fluctuations in the translational and rotational modes in the different directions vary by only about 20 %. This is primarily because the packing at high densities is primarily determined by steric effects, and not by the flow. The dense packing at high volume fractions results in a very efficient transport of energy between the different directions, and even though the 'temperature' is anisotropic, the anisotropy is numerically small, and it decreases as the volume fraction increases by more than 50 %. We also find that the temperature tends to a finite value in the close packing limit, even though the collision frequency diverges.

4.6. *Stress and dissipation rate*

One of the most important results obtained here is that the stress and the rate of dissipation of energy have the same divergence as the collision frequency as the limit of close packing is approached. There have been previous studies which have concluded that either the viscosity and the pressure diverge at different volume fractions (Khain & Meerson 2006; Khain 2007), or that the shear viscosity diverges with a power law different from that for the pressure (Bocquet, Errami & Lubensky 2002). The system considered by Khain (2007) was two-dimensional, and the difference in divergence was due to the constraints on shearing motion of a hexagonal close packed state. If a layer of particles is to slide relative to another fixed layer in two dimensions, it is necessary for the particles to have a significant displacement (approximately equal to 0.29 times the particle diameter) perpendicular to the direction of the mean velocity. This results in a greater resistance to shearing than to compression for large area fractions in two dimensions. In three directions, hexagonally close packed layers of particles can slide relative to each other in a zig-zag manner with a smaller perpendicular displacement, and so the difference in the volume fractions for the divergence of the viscosity and pressure is not as large.

There is an important distinction to be made regarding the divergence of the pressure and the viscosity. It is clear that for ordered states, the divergence of the shear viscosity in a shear flow will take place at a lower volume fraction than the divergence of the pressure in a system with no flow. From the rheological standpoint, the more relevant question is whether the divergence of the viscosity and pressure in a shear flow take place at different volume fractions; it is possible that even when there is ordering in two dimensions, the pressure and viscosity diverge at the same volume fraction *for a shear flow*, even though the pressure in the absence of shear diverges at a different volume fraction than the viscosity in the presence of shear. The present simulation studies show, quite clearly, that the pressure, viscosity and dissipation rate for a shear flow diverge at the same volume fraction. This is related to the fact that there is no icosahedral ordering in the shear flow, and so the arguments based on the presence of icosahedral ordering (or hexagonal ordering in two dimensions) do not apply in this case. We also find that the rate of divergence for pressure, viscosity and dissipation rate are the same, in contrast to the assumption made in the study of Bocquet *et al.* (2002).

The studies also showed that the Chapman–Enskog procedure using the Enskog approximation for the two-particle distribution function (Kumaran 2004, 2006*a*) do predict the correct qualitative behaviour for the stress and the dissipation rate, but the quantitative accuracy is poor for all values of the coefficient of restitution except $e_n = 0.9$. Reddy & Kumaran (2007), in their numerical comparisons for the case where $e_n = 0.9$, found good agreement between theory, event-driven and discrete-element simulations. This is an indication that the results obtained here are applicable not only to simulations which assume binary collisions between particles, but also to simulations where multi-body contacts are taken into account. However, the agreement between theory and simulations is poor for the cases where e_n is less than 0.9.

It was also observed that the prediction for the rate of dissipation of energy based on the Enskog approximation is also significantly larger than that observed in simulations. The agreement for the dissipation rate is reasonable for $e_n > 0.9$, but becomes poor as the coefficient of restitution is reduced below 0.9. This discrepancy was also observed in previous studies (Mitarai & Nakanishi 2005). This has motivated postulates (Jenkins 2006, 2007) that the mechanism for energy dissipation is different from that for stress transmission, and that it is necessary to introduce an additional length scale for the energy dissipation. However, the over-prediction of the dissipation rate does not provide the complete picture, because it is also found that a calculation based on the Enskog approximation under-predicts the collision frequency, as demonstrated by the significantly smaller prediction of the pair distribution function in figures 13 and 14. This has also been observed in previous studies (Goldschmidt, Beetstra & Kuipers 2002). Since the collision frequency is proportional to the first moment of the relative velocity distribution function of colliding particles, and the energy dissipation rate is proportional to the third moment, it must be concluded that the distribution function for the relative velocities is in error. Here, the distribution function for the relative velocities of colliding particles was examined to determine how the collision frequency, stress and dissipation rate are modified.

4.7. *Relative velocity distribution*

In a dense granular flow where the transport of momentum and energy occurs primarily due to particle collisions, the rate of transfer of momentum and energy depends on the distribution of relative velocities between colliding particles. In the Enskog approximation, the two-particle velocity distribution function is the product of the single-particle distributions and the pair distribution function at contact, and the relative velocity distribution turns out to be a Gaussian distribution, with variance two times that of the single-particle velocity distribution. In the present analysis, we resolved the distribution of relative velocity and angular velocity into two components, one along the line joining the centres w_n and the other perpendicular to the line joining the centres $\boldsymbol{w}_t$ and υ_t. It was found that the forms of the distributions for $\boldsymbol{w}_t$ and υ_t are close to Gaussian distributions. The 'temperature' for distribution of $\boldsymbol{w}_t$ shows little variation as the coefficient of restitution is decreased, and it has a value close to two times the translational temperature even at $e_n = 0.6$. The temperature for the distribution of υ_t does decrease to about 1.2 times the translational temperature at $e_n = 0.6$, though the form of the distribution function continues to be close to a Gaussian distribution. However, the distributions for $\boldsymbol{w}_t$ and υ_t have relevance only for the shear stress in rough particles, where the stress is influenced by the tangential impulse at the surfaces of contact; the collision frequency, normal stress and dissipation rate are not affected by the distribution of $\boldsymbol{w}_t$ and υ_t. Therefore, we

did not analyse these distributions further, and focused on the distribution of normal velocities w_n.

The distribution function for the normal velocities, $f_{w_n}(w_n)$, in a shear flow is anisotropic, since it depends on the angle between the line joining the centres and the flow direction. In order to take into account this anisotropy, the distribution function was expanded in a series in its spherical harmonic components. Even though the series has an infinite number of terms, it can be shown that there are only four non-zero contributions correct to second order in the strain rate in a simple shear flow. All of these components were analysed individually in some detail.

The term of largest magnitude in the spherical harmonic expansion is the spherically symmetric component $f^{(0)}_{wn}(w_n)$. For a fluid of elastic particles in the absence of flow, the spherically symmetric component is the only component in the expansion, and it can be shown that the distribution function for the normal velocities is a Maxwell–Boltzmann distribution with the temperature two times the translational temperature of the particles. For nearly elastic particles with $e_n = 0.98$, we find that the distribution function is close to a Gaussian distribution, but as the coefficient of restitution decreases below 0.8, we find from the simulations that the distribution function is an *exponential* distribution. The exponential form provides an excellent fit for rough particles; for smooth particles, the exponential form is in excellent agreement at low velocities, but there appears to be a transition to a slower decay at high velocities.

It should be noted that the relative velocity distribution function is an exponential distribution for low e_n, even though the distribution function of the particle velocities is close to a Gaussian. Kinetic theories (Sela & Goldhirsch 1998) calculate the correction to the single-particle velocity distribution due to the applied shear, and then use the Enskog approximation to express the two-particle distribution function as the product of the single-particle distribution functions. The more sophisticated theories (Lutsko 1996), which incorporate the effect of shear on the structure, consider the pair distribution function to be anisotropic, but still use the molecular chaos approximation for the pre-collisional velocities. Here, we find that the two-particle distribution is very different from the product of the single-particle distributions, even for the pre-collisional velocities. The molecular chaos assumption is not applicable, and there are significant correlations in the velocities of colliding particles. We also propose a method for incorporating these correlations by directly modelling the relative velocity distribution, which is responsible for the transmission of collisional stresses.

The reason for the exponential distribution in dense flows is not difficult to understand. In dense hard or soft particle systems, it is known that particles are confined in a 'cage' formed by surrounding particles, and diffusion takes place by rare cage-breaking events, where a particle jumps to a neighbouring cage. A similar procedure takes place in shear flow, except that the mean shear is likely to aid the cage-breaking procedure, so that the escape events become more frequent as the mean strain rate increases. However, in a shear flow, there is an additional effect, which is that if a particle is displaced across streamlines when it jumps to a neighbouring cage, the mean velocity of the surrounding particles in the new location is different from the mean velocity in the original location. Due to this, the particle experiences a larger fluctuation in the impulse from the surrounding particles. This fluctuation decays due to inelastic collisions till the particle velocity distribution equilibrates to the mean velocity at the new location. This results in rare large fluctuations in the velocity of the particles, and gives rise to a slower-than-Gaussian decay of the velocity distribution function.

Though the form of the distribution function is relatively easy to rationalize, the coefficients in the distribution function will be more difficult to obtain from first principles. Here, we have obtained fitting relations for the parameter α in the exponential distribution $f_{wn}^{(0)} = \alpha \exp(-\alpha w_n)$. It is found that α diverges as the volume fraction approaches the close packing volume fraction for a given coefficient of restitution. This divergence is expected, since we anticipate that the particles will all come to rest at the close packing volume fraction, in which the distribution function for relative velocities is a delta function at $w_n = 0$. Based on the data available, the best fit we can infer for the form of the divergence turns out to be log divergence for rough particles, and a power law divergence for smooth particles. The reason for the difference in the divergence behaviour is not clear.

In order to obtain a uniform approximation for the distribution function for all coefficients of restitution, a composite distribution function was postulated. This is a linear combination of an exponential and a Gaussian distribution, with the weights of the two components adjusted to reduce the difference between the composite distribution and the actual distribution functions. The parameters in the composite distribution were evaluated as a function of volume fraction and coefficient of restitution, and this composite distribution was further used to study the pressure and rate of dissipation of energy.

The other spherical harmonic components of the distribution function, $f_{wn}^{(1)}$, $f_{wn}^{(2)}$ and $f_{wn}^{(3)}$ were also analysed. It was found that these components have a form that is similar to that of $f_{wn}^{(0)}$, and the variation of the ratios $(f_{wn}^{(1)}/f_{wn}^{(0)})$, $(f_{wn}^{(2)}/f_{wn}^{(0)})$ and $(f_{wn}^{(3)}/f_{wn}^{(0)})$ with w_n is small compared to the variation of $f_{wn}^{(0)}$ itself. One of the implications of this is that the Enskog approximation (the two-particle velocity distribution function is the product of the single-particle velocity distributions of the colliding particles and the pair distribution function) is not a good approximation; if the Enskog approximation were valid, then we would have found that $(f_{wn}^{(1)}/f_{wn}^{(0)}) \propto w_n$ for e_n close to 1. For low values $e_n = 0.6$, the Enskog approximation would predict that the ratio $(f_{wn}^{(1)}/f_{wn}^{(0)})$ is independent of w_n; however, the value predicted by the Enskog approximation is more than an order of magnitude larger than that obtained from simulations. This leads us to conclude that the Enskog approximation is uniformly poor for all values of the coefficient of restitution in dense flows. The constant distribution ratio indicates some self-similarity in the evolution of the different spherical-harmonic components of the distribution function which deserves further study.

The pressure and the dissipation rates were calculated using the model for the distribution of relative velocities. The shear stress was obtained from the dissipation rate using the energy balance condition. It was found that there is quantitative agreement between the theoretical results based on the composite distribution and the simulation results for the pressure and dissipation rate. The agreement is within 1 % in the case of rough particles, since we found that the exponential distribution is an excellent fit for the relative velocity distribution. The agreement is a little poorer, within 5 %, for smooth particles, possibly because the slower decay in the tail of the distribution is not well captured by the composite distribution. In any case, the agreement is much better than the predictions obtained using the Chapman–Enskog procedure and the Enskog approximation for the pair distribution function, which are in error by an order of magnitude or more for the dissipation rate at the lowest coefficient of restitution $e_n = 0.6$.

For smooth particles, the spherical harmonic component $f_{wn}^{(1)}$ can be used to evaluate the shear stress. In the case of rough particles, there is an additional component to the stress due to the tangential impulse at the surface of contact. In the simulations,

it is found that the component due to the tangential component of the impulse is numerically small, and the shear stress due to the normal impulse constitutes between 80 % and 90 % of the total shear stress. Therefore, it is possible to obtain the shear stress within an accuracy of 10 %–20 % by just considering the normal component of the impulse during particle collisions.

The shear stress due to the normal impulse at contact was evaluated using the approximation that $(f_{wn}^{(1)}/f_{wn}^{(0)})$ is a constant. Quantitative agreement was found to within 15 % for smooth particles; the agreement for rough particles was even better. The approximations for $(f_{wn}^{(2)}/f_{wn}^{(0)})$ and $(f_{wn}^{(3)}/f_{wn}^{(0)})$ were used to obtain the first- and second-normal stress differences as well.

4.8. *Relation to soft particle studies*

The calculation carried out here, which is restricted to hard particles, needs to be placed in the context of real granular flows, which have a finite particle stiffness. For definiteness, let us consider the flow down an inclined plane. At high angles of inclination, when the density is low, the particle interactions will be dominated by binary collisions. In this case, by dimensional analysis, all the stress components scale as the square of the strain rate, since the period of interaction does not affect the dynamics. As the angle of inclination decreases or the density increases, the system will transition into a multi-body contact regime, where the finite stiffness of the particles does affect the dynamics. When the angle is further decreased, the flow will stop and the density will assume the limiting value it has in a static state. The volume fraction at which there is a transition from the binary to the multi-body contact regime will depend on the particle stiffness. For very stiff particles, the transition will be at a higher volume fraction (lower angle of inclination), whereas for softer particles, the transition will take place at a lower volume fraction (higher angle of inclination).

There are different measures of the volume fraction (or angle of inclination) range for which the binary contact regime is encountered, such as the average collision time (Campbell 2005) and the contact lifetime distribution (Silbert *et al.* 2007). Another indirect measure is from the stress law for a steady shear flow; dimensional analysis indicates that the stress is proportional to the square of the strain rate in the binary contact regime, whereas it is independent of strain rate for a very dense flow with multi-body frictional contacts. The simplest measure is probably the co-ordination number, which is the number of particles which are simultaneously in contact. This co-ordination number was analysed as a function of angle of inclination and volume fraction by Reddy & Kumaran (2007) in three dimensions. The calculations were carried out using the DEM simulation technique for a system whose angle of repose is approximately $\theta = 21^\circ$, and which has a stable flow regime in the range $21^\circ \leqslant \theta \leqslant 25^\circ$. The results indicated that for relatively soft particles of the type first analysed by Silbert *et al.* (2001), the co-ordination number is larger than 1 for $\theta \leqslant 24^\circ$. However, if the spring stiffness was increased to correspond to real materials such as sand or glass beads, the co-ordination number decreases more rapidly with angle of inclination, and is less than 1 for $\theta \geqslant 22^\circ$. Thus, the multi-body contact regime is encountered for over a range of less than 1° of inclination for real materials, and the system rapidly transitions to a binary contact regime.

In the present analysis, we deal exclusively with hard-particle systems which have infinite spring stiffness, and so the particle interactions are considered to be binary collisions. So the present calculation can capture the binary collision regime, but not the multi-body contact regime, and so it is important to place the present results in

the context of real granular flows with finite stiffness. We find, for example, that the collision frequency (scaled by the inverse of the strain rate) increases as the volume fraction is increased, and it diverges at a finite volume fraction ϕ_{ad}. For particles with finite stiffness, the collision frequency will deviate from the hard-particle value when the system transitions to a multi-body contact regime, and the divergence of the collision frequency will be cutoff at this volume fraction. The volume fraction at which this deviation occurs will increase as the particle stiffness is increased, and so the present calculation provides an upper limit for the collision frequency for real granular flows. As particle stiffness is increased, there will be a smaller and smaller range of volume fractions (or angles of inclination) in the multi-body regime for which there is a deviation from the hard-particle results. As discussed above, the simulations of Reddy & Kumaran (2007) indicate that this range is less than 1° for real materials such as sand and glass. The present simulations provide quantitative results for the collision frequency, stress and dissipation rate outside this multi-body regime where binary contacts dominate.

It should be noted that the divergence of the collision frequency is not a simulation artefact. Even for monodisperse elastic hard spheres in the absence of shear, there is a divergence of the collision frequency at the random close packing volume fraction. This divergence is usually expressed as a divergence of the pair distribution function χ (Torquato 1995), but the two are equivalent, since the collision frequency is $(2\sqrt{\pi}\rho^2\chi\sqrt{T})$, where T is the translational temperature. Note that the divergence of the collision frequency occurs at a constant temperature as the volume fraction is changed. (Since there is no molecular energy scale in a hard-sphere fluid, the temperature just sets the scale for the fluctuating velocity of the particles, and does not induce any phase transitions.) Here, we are analysing how this divergence is affected by the imposed shear.

The divergence of the collision frequency in the hard-particle model also has an important implication for real granular materials which have finite stiffness. Since it is not possible to access volume fractions greater than ϕ_{ad} in the hard-particle model, the implication is that the system has to be in the multi-body contact regime for $\phi > \phi_{ad}$. Of course, the curves for the collision frequency (or pressure, viscosity, etc.) versus volume fraction will depart from the limiting curves for the hard-particle model even for $\phi < \phi_{ad}$, but the departure will decrease as the spring constant is increased. We will discuss the various estimates of this volume fraction range a little later. However, it is important to note here that the hard-particle limit for the variation of collision frequency, pressure, stress and dissipation rate with volume fraction is relatively easy to obtain by extrapolating the results of hard-particle simulations. It would be much more difficult to obtain by using soft-particle simulations and increasing the spring stiffness systematically, because the simulation time step decreases as the spring stiffness increases, and it requires prohibitively long computational times to simulate particles with stiffness corresponding to sand and glass beads. This is one reason why many of the simulations (notably Silbert *et al.* 2001) are carried out with particles whose stiffnesses are about four orders of magnitude smaller than sand particles or glass beads.

One of the persistent puzzles that has arisen out of previous large-scale simulations on chute flows is that the results for the stresses obtained do not vary much as the spring stiffness is decreased, and the system transitions from a binary contact regime to a multi-body contact regime. This was first observed by Silbert *et al.* (2001), and was later confirmed by Reddy & Kumaran (2007). The latter also reported that the results for the stress at constant volume fraction from binary contact event-driven

simulations are in numerical agreement with those for DEM simulations at the same volume fraction even when the particles have multiple contacts in the DEM simulations. The reasons for this are not established yet, but one reason investigated by Reddy & Kumaran (2007) is that even when there are multiple contacts between particles, there is one contact which has the largest force. This indicates that the results obtained from a hard-particle model may have significance even when the system is in the multi-body contact regime. A similar observation was made for equilibrium liquids such as water, where it was found that the Chapman–Enskog procedure using the Enskog approximation for the pair distribution function provides dynamical properties correct to within about 25 %–30 % of experimentally measured values (Theodosopulu & Dahler 1974*a*, *b*).

This indicates that there are two different issues here, the first is whether the system is actually in the binary contact regime, and the second is whether the numerical predictions of a hard-sphere calculations provide quantitative estimates for a granular material composed of soft particles in the binary contact regime. We first examine the former, which requires the estimation of the appropriate numerical values for the spring constants for contacts between particles. There are considerable differences for the spring constants assumed for sand particles, for example, in literature. It is known that real contacts between smooth particles have a Hertzian force law, where the restoring force is proportional to the square root of the overlap between particles. However, it is more convenient to use a Hookean (linear) contact model between particles in simulations. If we assume that the spring constant depends only on the particle diameter and the elasticity modulus of the material, then the spring stiffness for the linear model can be estimated as $k_n \sim (Ed)$, while that for the Hertzian model can be estimated as $k_n \sim (Ed^{1/2})$, where E is the elasticity modulus and d is the particle diameter. If we assume an estimate of the elasticity modulus of $10^{11}\,\mathrm{N\,m^2}$ appropriate for sand and glass, the spring constant for the linear model is in the range $k_n \sim 10^7$–$10^8\,\mathrm{N\,m^{-1}}$ for particles with diameter in the range 100 μm–1 mm, while the spring constant for the Hertzian model is in the range $k_n \sim 10^9$–$10^{10}\,\mathrm{N\,m^{-3/2}}$. There have been recent experiments by Cole & Peters (2007, 2008) which report that for smooth particles, the spring constant is very well approximated (to within 20 %) by the Hertzian contact law. A more interesting finding is that even though a Hertzian model is more appropriate for contacts between smooth particles, the contacts between sand grains are, in fact, linear, due to the asperities on the grains. For a range of particle diameters (0.2–2 mm), Cole & Peters (2007) find that the spring stiffness is in the range of $10^6\,\mathrm{N\,m^{-1}}$. This is about two orders of magnitude higher than the estimate of Campbell (2005), where the spring constant (based on the speed of sound in loose sand) is assumed to be of the order of $10^4\,\mathrm{N\,m^{-1}}$, though it is about an order of magnitude lower than the value of $10^7\,\mathrm{N\,m^{-1}}$ obtained based on the material elasticity modulus for 100 μm particles. This difference in estimates leads to differing conclusions when the dimensionless numbers used in simulations are transformed into dimensional numbers for real systems. In particular, the under-estimation of the spring constant by two orders of magnitude by Campbell (2005, 2006) also leads to an over-estimation, by 1–2 orders of magnitude, of the minimum strain rate for which the binary collision approximation is valid.

The differences in the interpretation of constant volume simulations are relatively easily resolved. The Discrete Element simulations of Campbell (2002) show that the system undergoes a transition to the multi-body regime when the volume fraction is increased beyond about 59 %. This is in agreement with the results of the present simulations, which show that in a sheared simulation of hard particles, the collision

frequency diverges at a volume fraction between 58 % and 59 % for sufficiently inelastic particles. Simulations of flows down an inclined plane (Silbert *et al.* 2001; Reddy & Kumaran 2007) also find that the volume fraction in the flow does not exceed 59 % even at the lowest angle of inclination, even though the random close packing volume fraction for elastic spheres is 64 %. All of these results indicate that the volume fraction for dynamical arrest for sheared inelastic particles needs to be defined as the volume fraction at which the collision frequency diverges *in the sheared state*, and this volume fraction is a function of the coefficients of restitution, as shown in the present analysis. Once this is done, then all the results are consistent with each other. In constant volume simulations, the system undergoes a transition to a multi-body contact regime at a volume fraction of about 59 %, beyond which stress transmission is by contact forces between particles which are transmitted presumably by 'force chains'. However, force chains require compressive forces at both ends. Since there cannot be a compressive force at the free surface of an inclined plane flow, the flow expands such that volume fraction does not exceed about 59 %.

The constant stress simulations (Campbell 2005) are more difficult to reconcile with the inclined plane simulations. A part of the reason is that the inclined plane flow is not a constant stress flow, but is actually a constant volume fraction flow in which the stresses increase linearly with height. This is because the volume fraction in the bulk of the flow is remarkably constant, as shown by the pioneering work of Silbert *et al.* (2001). This is a consequence of the constant ratio of shear and normal stresses in the bulk (Kumaran 2008), and their linear variation with height in the bulk. Due to this, it may be more appropriate to compare the inclined plane simulations with constant volume fraction simulations. There is one equivalence which is easily apparent, which is that the limiting low stress critical state in the simulations of Campbell (2005) would correspond to the volume fraction at which the collision frequency diverges in the present simulations; this volume fraction is found to decrease from 0.62 to about 0.58 as the dissipation is increased in both studies. The other equivalences are less clear, probably because different quantities are being measured to infer the presence of multi-body contacts. On the basis of average contact time between particles, Campbell (2005) concludes that the system is in the multi-body contact regime, whereas on the basis of the contact lifetime distribution, Silbert *et al.* (2007) infer that the dominant stress transmission mechanism is due to short-lived contacts with large impulses. Both of these measures could be simultaneously correct if the distribution function for the contact lifetime has an appropriate form, where the stress transmission is dominated by rare short-lived contacts with large forces, while the average contact time is dominated by long-lived contacts with small force. It is necessary to examine not just the contact lifetime, but also the distribution of forces in contacts. Another measure used is the ratio of shear and normal stresses, and the expectation that this should be a constant when the Bagnold law is satisfied for collisional flows. However, the volume fraction is changing in the constant stress simulations, and the ratio of stresses may not be a constant due to the variation in volume fraction. Reddy & Kumaran (2007) considered the forces on a single particle, and measured the ratio of the second largest and the largest forces in magnitude. They found that this ratio is quite small even in the multi-body contact regime; this is in contrast to the force chain picture where the particles are held in contact by nearly equal and opposite forces along the line of contact. More work needs to be done to clarify these issues.

Another simulation procedure used for dense granular flows is the contact dynamics simulations (Lois, Lemaitre & Carlson 2005). This is a combination of event-driven and molecular dynamics simulations; the simulations are advanced in constant time

steps, and all particles which collide within one time interval are considered to be in simultaneous contact. The stresses transmitted by these particles are called 'contact stresses', in contrast to collisional stresses. The definition of collisional and contact stresses is clearly subjective, since it depends on the time interval used for advancement. This subjectivity is more acute in a regime where the collision frequency is diverging. As the volume fraction is increased and the collision frequency increases, there will be more and more particles colliding within a fixed time interval, and this will result in more particles considered to be in simultaneous contact. This is an artefact of the finite time step of the simulation; if the simulation time step is made sufficiently small (much smaller than the inverse of the collision frequency), there will be only one collision per time interval, and there will be no contact stresses. It is necessary to carry out simulations in which the period of the simulation time step is decreased in proportion to the inverse of the collision frequency, in order to examine whether the system is actually going from the binary contact to the multi-body collision regime.

Finally, an issue of vigorous debate in soft-particle systems is the 'jamming transition' and the 'jamming phase diagram' (Liu & Nagel 1998). An analogy is drawn between the glass transition in thermal systems and the jamming transition in dissipative systems, by depicting a boundary in the (1/density)–temperature–shear (stress or rate) three-dimensional coordinate system. In our interpretation here, the point at which the collision frequency diverges for a hard-particle system is the point at which the system has to transition to an extended contact (finite elasticity modulus) regime for particles of large but finite stiffness. While studying the jamming transition, one usually moves in the direction of decreasing the density from a static state until the particles are no longer in permanent contact. Therefore, for a hard-particle system, the jamming volume fraction should be the volume fraction at which the collision frequency diverges, and beyond which the particles have to be in extended contact. However, the variables used to describe the jamming point will be different for hard-particle systems. Since there is no energy scale for the particle interactions, the time dimension can be scaled by the inverse of the strain rate, and the jamming volume fraction will not depend on strain rate; it will depend only on the coefficients of restitution which characterize the inter-particle interaction. In this interpretation, the volume fraction for 'jamming' decreases as the coefficients of restitution is decreased, or the collisional dissipation is increased. In the limit of elastic collisions ($e_n = 1$), the 'jamming' volume fraction would correspond to the random close packing volume fraction $\phi_c = 0.64$. As the coefficient of restitution is decreased, the volume fraction for arrested dynamics, ϕ_{ad}, decreases to a value of about 0.58 for highly inelastic particles. Therefore, if the inverse of the density is plotted as a function of $(1 - e_n)$, the curve would have an upward curvature around $(1 - e_n) = 0$, and approach a constant value as e_n decreases below about 0.8. This is in contrast to the downward curvature about the shear axis, and the decrease in (1/density) to zero at finite shear rates, which is usually depicted (Liu & Nagel 1998).

4.9. *Flow down an inclined plane*

The models for the pressure and shear stress were used to predict the angle of repose for the flow down an inclined plane. It was found that in the range $0.6 \leqslant e_n \leqslant 0.8$, the angle of repose predicted by the model is about 21°. This is slightly higher than the value close to 20° observed in simulations (Silbert *et al.* 2001). The discrepancy may be because the model is based on simulations of relatively small size; an increase in the size of the simulations may slightly alter the numerical values of the ratio of

shear stress and pressure. The discrepancy could also be because the binary contact regime is only valid upto an angle of inclination of 21°, and the flow in the range 20°–21° could be in the multi-body contact regime. Similarly, the angle of inclination is predicted to be in the range 24°–25° for the lowest volume fractions of around $\phi = 0.54$ which could be attained in simulations; this is also in quantitative agreement.

The present study complements an earlier analysis (Kumaran 2008), where the constitutive relations obtained using the Chapman–Enskog procedure based on the Enskog approximation for the pair distribution function were used to analyse the granular flow down an inclined plane. There, it was shown that all the features of the flow were captured by the constitutive models. However, there was quantitative disagreement in the prediction of the angle of repose, as well as in the variation of the volume fraction with the angle of inclination. It was already anticipated in Kumaran (2008) and Reddy & Kumaran (2007) that a part of the disagreement is because the pair distribution function for a shear flow of inelastic particles is different from that for elastic particles at equilibrium in the absence of shear; the latter is often used in literature for quantitative predictions of the stresses in shear flows. It was also anticipated (Kumaran 2008) that the Enskog approximation may be in error because there are strong correlations in the velocities of colliding particles. The objective of the present analysis was to correct these deficiencies. We have determined the form of the collision frequency in the dense limit, and obtained the distribution function for the pre-collisional relative velocity of colliding particles, and incorporated these into the constitutive relations for dense shear flows of inelastic particles. The results are in quantitative agreement for the angle of repose and the variation of volume fraction with angle of inclination for the flow down an inclined plane. This definitively shows that the constitutive relations for the shear flow of inelastic particles obtained using the binary collision approximation are valid for dense granular flows of practical interest.

The present analysis is valid only when contacts are instantaneous; this leads to a Bagnold form for the stress–strain relationship. To the extent that the Bagnold law is satisfied in real systems such as chute flows, this analysis provides a way of calculating the stress–strain rate relationship for these flows. The purpose is to provide constitutive models that can actually be used to calculate coefficients which can then be used in practical applications. Of course, one would expect that as the angle of inclination is decreased, the system goes into a multiple contact regime and then stops. The present analysis will not be applicable in the multiple contact regime, but simulations discussed above have shown that this regime is small, at least for chute flows. The present analysis provides the transition from binary to multi-body contact regime as the point at which the collision frequency diverges; to the extent that this is close to the angle at which flow stops, this would provide a good numerical estimate of the angle or repose, as well as the Bagnold coefficients.

A lot of work has been done in trying to account for about particle correlations, force networks, force chains, etc. in systems with multi-body contacts. Though these studies classify flow domains into various regions in which inertial dominates, elasticity dominates, etc. (Campbell 2006), there are no calculations of constitutive relations. It is fair to say that at present, no calculation, apart from those based on kinetic theory (Kumaran 2008), can even predict the slope of the variation of angle of inclination with volume fraction. Apart from classification, there are often references to force chains and force networks, which are very qualitative, and which are not ultimately connected to the stress values (Campbell 2002, 2005). We can get quantitative measures of the stress transmitted by force chains only if we can quantitatively define a force chain,

and show that most of the stress in a sample is actually transmitted in a force chains. Therefore, for the concept of force chains to be useful in practical calculations, there needs to be some consensus evolved on fundamental issues, such as whether a force chain has to have a compressive stress on both sides due to bounding surfaces (this is clearly not present in flows with a free surface), or whether it can just disappear into a free surface. System size dependence is another important unresolved aspect, and it is important to determine whether the dynamics of the force chain is independent of system size. If the dynamics does depend on system size and boundary conditions, the rheology is not local, and one cannot write constitutive relations in terms of gradients of hydrodynamic fields. If it does not depend on system size, there needs to be some conceptual understanding of the meaning of force chains in an infinite system, with regard to whether they are sample spanning or not. Perhaps renormalization procedures developed in the study of critical phenomena would be of some use.

The same is true with the concept of percolating force networks. In a flowing material, the network has to be transient, so it is necessary to specify if there is a percolating network at all times, or only some of the time. The dependence of the percolation threshold on spring stiffness and system size are important issues. An important question is the applicability of percolation network models to open systems such as chute flows, where there is one stress-free boundary at which there is no stress on the system. Another conceptual question is that one can obtain constitutive equations only if the rheology is local, whereas in percolating networks the rheology is not local, because the network spans the system. It would be necessary to define other additional parameters, such as the force distribution in a network or in a force chain, and write gain–loss equations for these. These other order parameters would then coupled to the momentum equation. The gain–loss equations would involve rate constants, and it is not clear how one would obtain these, and whether quantitative comparisons can be made without fitting parameters.

In a phenomenological description of the rheology (GDR MiDi 2004), the ratio of the shear and normal stress is expressed in terms of the I parameter, which is the ratio of the strain rate and the square root of the normal stress (suitably scaled by particle mass and diameter to make the ratio dimensionless). This is a useful approximation, since it seems to collapse the data for a range of experimental situations, though it should be noted that it does not collapse data near walls where temperature boundary layers (Kumaran 2008) are present. However, this does not qualify as a valid rheological model for the following reason. The purpose of a rheological model is to calculate all components of the stress in terms of the the rate of strain or its derivatives, not to calculate one component of the stress in terms of another. A flowing material is described by the mass and momentum conservation equations (energy is not conserved in the present system). In the momentum conservation equation, there is a momentum flux (stress tensor) which has to be related to the field variables (density and velocity) and their gradients by the constitutive relation. While the I parameter description may be useful for yield criteria, it cannot be directly inserted into mass and momentum conservation equations to obtain a closed set of governing equations for the density and velocity fields.

There have been some theories which attempt to obtain the ratio of stresses from correlations (Ertas & Halsey 2002). Motivated by the observation of Pouliquen (1999) that there is a connection between the average velocity in the flowing state of a granular material and the minimum height h_{stop} required to sustain a flow. These studies postulate that there is a correlation length within the flow which is of order h_{stop}. There are many ad-hoc approximations in these theories, such as the calculation

of times for the time taken for inelastic collapse, or a vortex rotation time in the flow. If these structures do exist in the flow, then it should be relatively easy to verify from simulations, since the positions and velocities of all particles are available from the simulation results. There is, as yet, no evidence that these structures are actually observed in simulations, and recent calculations (Baran *et al.* 2006) conclude that particle motion is correlated over relatively short distances of the order of one-particle diameter, and this distance does not increase proportionally to h_{stop}.

Another correlation effect that has been postulated is the decrease in the dissipation rate (but not the stresses) due to correlations (Jenkins 2006, 2007). This is motivated by event-driven (Mitarai & Nakanishi 2005) and contact dynamics (Lois *et al.* 2005) simulations which showed that while the stress is well predicted by expressions from kinetic theory, the dissipation rate is smaller than that predicted by kinetic theory. Lois *et al.* (2005) also modified the energy equation by postulating an additional parameter in the energy equation, and obtained this parameter on the basis of a shear transformation zone theory. However, the dissipation rate alone does not provide the complete picture, because it has also been found that the frequency of collisions is higher than that predicted by kinetic theory in dense flows (Goldschmidt *et al.* 2002). The present study shows that there is a change in the form of the relative velocity distribution, from a Gaussian to an exponential form. Once this is incorporated in the theory, numerically accurate results are obtained for the collision frequency, stress and the dissipation rate, without the need for postulating correlations.

While postulating that there are correlations in the flow, it is important to make a definite conclusion about whether the rheology is local or not. The rheological model will be valid only if the thickness of the differential volume considered is larger than the correlation length; if it is smaller than the correlation length, its surface would break though a chain of particles or an eddy, and the stress response would depend on the dimensions of the volume considered. If the length scale is comparable to the correlation length, then one cannot do a gradient expansion in the ratio of the microscopic (correlation) length and the macroscopic length, and so it is not possible to write constitutive relations. When the correlation length diverges it should be comparable to the system size at some point, and at this point the assumption of local rheology is invalid. This is the same reason why eddy viscosity models for turbulence do not have a rigorous basis.

In the kinetic theory calculations based on binary interactions (Kumaran 2004, 2006*a*, *b*, *c*), a constitutive relation for the stress tensor is explicitly calculated. It predicts all the qualitative features of the flow down an inclined plane.

(*a*) It does predict the minimum angle at which the flow of hard-spherical particles would stop, as the angle at which the collision frequency and the Bagnold coefficients diverge. Since the Bagnold coefficients diverge and the gravitational force density does not change much, the strain rate decreases to zero. It has commonly been assumed (Campbell 2006) that since kinetic theories treat a granular material as a viscous fluid, these theories cannot predict a yield condition. This is erroneous, because the granular material does not have equilibrium thermal fluctuations, and the particles are fluidised only when there is an energy source. For a homogeneous granular flow, there is a coupling between the shear production and the inelastic dissipation of energy. A flowing state is possible only when the rate of production due to shear is sufficient to overcome the rate of dissipation due to inelastic collisions. As the angle of inclination is decreased, the component of the gravitational force along the plane decreases, and the rate of shear production decreases. At some minimum angle, the rate of shear production is not sufficient to overcome the rate of inelastic dissipation,

and the flow stops. Thus, it is possible to obtain a macroscopic yield criterion without any microscopic yield condition or yield stress.

(*b*) In addition, constitutive relations obtained by the Chapman–Enskog procedure using the Enskog approximation for the pair distribution function correctly predict the qualitative features of the stress tensor if the coefficients are derived using the rough particle model and the Burnett coefficients are included; the first normal stress is found to be negligible and could be positive or negative, while the second normal stress difference is much larger and positive. The correct slope of the volume fraction angle of inclination curve, required for stability, is also obtained if a rough particle model is used for binary interactions. Though the slope required for stability is obtained, the numerical values of the angle of inclination are not in quantitative agreement. The purpose of this paper (Part II of the present analysis) is to examine the reasons for this. We find that distribution of the pre-collisional relative velocities is not a Gaussian, but approaches an exponential as the coefficient of restitution is decreased. Once this is incorporated, we are able to quantitatively predict the volume fraction as a function of the angle of inclination.

(*c*) Simulations show that the dynamics of the flow in thin regions at the top and bottom is different from that in the bulk (Silbert *et al.* 2001). The temperature conditions at the boundary are known to have virtually no effect on the bulk flow. Most theories either do not have a boundary layer length scale, or assume that it is the same as the correlation length. A major advantage of kinetic theory is that it does predict a boundary length scale, which is the conduction length. This length is obtained without having to make assumptions about correlations lengths, force chains, etc. When this is small compared to the height of the flow, there is a balance between shear production and viscous dissipation in the bulk. The conduction term becomes important only in thin boundary layers at the top and bottom. Analytical solutions are possible for these in the high-density limit (Kumaran 2008), and solvability conditions for the boundary layer equations can also be derived. The theory naturally predicts that the conditions at the boundary do not affect the flow in the bulk; this result is not obtained from other correlation-length theories.

(*d*) Most theories assume that the minimum height required for a flowing layer (h_{stop}) is the same as the correlation length in the flow, but this is equivalent to assuming the physical mechanism at the beginning of the calculation. In contrast, the present theory is able to qualitatively predict the variation of volume fraction with angle of inclination for an infinite flow, as well as the variation of the minimum height (h_{stop}) with angle of inclination, without having to invoke a correlation length at the beginning of the calculation. It also qualitatively provides the variation of h_{stop} with angle of inclination for a dissipative base, and predicts that $h_{stop} = 0$ if the base is energetic (injects energy into the flow).

In summary, in the earlier analysis (Kumaran 2008), it was noted that though all the qualitative features are accurately predicted, there are numerical differences. In the present analysis, we have identified the source of these differences, and shown how these can be corrected, to obtain quantitative predictions for the dynamics of the flow down an inclined plane.

This research was supported by the J. C. Bose Fellowship, Department of Science and Technology, Government of India. The author would like to thank Mr K. Anki Reddy for help with some of the simulations.

REFERENCES

Baran, O., Ertas, D., Halsey, T. C., Grest, G. S. & Lechman, J. B. 2006 Velocity correlations in dense gravity-driven granular chute flow. *Phys. Rev.* E **74**, 051302.

Bocquet, L., Errami, J. & Lubensky, T. C. 2002 Hydrodynamic model for a dynamical jammed-to-flowing transition in gravity driven granular media. *Phys. Rev. Lett.* **89**, 184301–184304.

Campbell, C. S. 1997 Self-diffusion in granular shear flows. *J. Fluid Mech.* **348**, 85–101.

Campbell, C. S. 2002 Granular shear flows at the elastic limit. *J. Fluid Mech.* **465**, 261–291.

Campbell, C. S. 2005 Stress-controlled elastic granular shear flows. *J. Fluid Mech.* **539**, 273–297.

Campbell, C. S. 2006 Granular material flows – An overview. *Powder Tech.* **162**, 208–229.

Chapman, S. & Cowling, T. G. 1970 *The Mathematical Theory of Non-Uniform Gases.* Cambridge University Press.

Cole, D. M. & Peters, J. F. 2007 A physically based approach to granular media mechanics: grain-scale experiments, initial results and implications to numerical modelling. *Granular Matter* **9**, 309–321.

Cole, D. M. & Peters, J. F. 2008 Grain-scale mechanics of geologic materials and lunar simulants under normal loading. *Granular Matter* **10**, 171–185.

Delannay, R., Louge, M., Richard, P., Taberlet, N. & Valance, A. 2007 Towards a theoretical picture of dense granular flows down inclines. *Nature Mater.* **6**, 99–108.

Dorfman, J. R. & Cohen, E. G. 1972 Velocity-correlation functions in two and three dimensions: low density. *Phys. Rev.* A **6**, 776.

Dufty, J. 1984 Diffusion in shear flow. *Phys. Rev.* A, **30**, 1465–1476.

Ernst, M. H., Cichocki, B., Dorfman, J. R., Sharma, J. & van Beijeren, H. 1978 Kinetic theory of nonlinear viscous flow in two and three dimensions. *J. Stat. Phys.* **18**, 237–270.

Ertas, D. & Halsey, T. C. 2002 Granular gravitational collapse and chute flow. *Europhys. Lett.* **60**, 931–937.

Foerster, S. F., Louge, M. Y., Chang, H. & Allia, K. 1994 Measurements of the collision properties of small spheres. *Phys. Fluids* **6**, 1108–1115.

Foss, D. R. & Brady, J. F. 2000 Structure, diffusion and rheology of Brownian suspensions by Stokesian Dynamics simulation. *J. Fluid Mech.* **407**, 167–200.

Garzo, V. & Dufty, J. 1999 Dense fluid transport for inelastic hard spheres. *Phys. Rev.* E **59**, 5895.

GDR MiDi 2004 On dense granular flows. *Euro. Phys. J.* E **14**, 341–365.

Goldschmidt, M. J. V., Beetstra, R. & Kuipers, J. A. M. 2002 Hydrodynamic modelling of dense gas-fluidised beds: comparison of the kinetic theory of granular flow with three-dimensional hard-sphere discrete particle simulations. *Chem. Engng Sci.* **57**, 2059–2075.

Jenkins, J. T. 2006 Dense shearing flows of inelastic disks. *Phys. Fluids* **18**, 103307.

Jenkins, J. T. 2007 Dense inclined flows of inelastic spheres. *Granular Matter* **10**, 47–52.

Khain, E. 2007 Hydrodynamics of fluid–solid coexistence in dense shear granular flow. *Phys. Rev.* E **75**, 051310.

Khain, E. & Meerson, B. 2006 Shear-induced crystallization of a dense rapid granular flow: hydrodynamics beyond the melting point. *Phys. Rev.* E **73**, 061301.

Kirkpatrick, T. R. & Nieuwoudt, J. 1986 Stability analysis of a dense hard-sphere fluid subjected to large shear-induced ordering. *Phys. Rev. Lett.* **56**, 885–888.

Kumar, V. S. & Kumaran, V. 2006 Bond-orientational analysis of hard-disk and hard-sphere structures. *J. Chem. Phys.* **124**, 204508.

Kumaran, V. 1998 Temperature of a granular material fluidised by external vibrations. *Phys. Rev.* E **57**, 5660–5664.

Kumaran, V. 2004 Constitutive relations and linear stability of a sheared granular flow. *J. Fluid Mech.* **506**, 1–43.

Kumaran, V. 2006*a* The constitutive relations for the granular flow of rough particles, and its application to the flow down an inclined plane. *J. Fluid Mech.* **561**, 1–42.

Kumaran, V. 2006*b* Kinetic theory for the density plateau in the granular flow down an inclined plane. *Europhys. Lett.* **73**, 1–7.

Kumaran, V. 2006*c* Velocity autocorrelations and the viscosity renormalisation in sheared granular flows. *Phys. Rev. Lett.* **96**, 258002–258005.

Kumaran, V. 2008 Dense granular flows down an inclined plane – from kinetic theory to granular dynamic. *J. Fluid Mech.* **599**, 121–168.

Kumaran, V. 2009*a* Dynamics of a dilute sheared inelastic fluid. I. Hydrodynamic modes and the velocity correlation functions. *Phys. Rev.* E **79**, 011301.

Kumaran, V. 2009*b* Dynamics of a dilute sheared inelastic fluid. II. The effect of correlations. *Phys. Rev.* E **79**, 011302.

Lahiri, R. & Ramaswamy, S. 1994 Shear-Induced melting and re-entrance: A model. *Phys. Rev. Lett.* **73**, 1043–1046.

Liu, A. J. & Nagel, S. R. 1998 Jamming is not just cool anymore. *Nature* **396**, 21–22.

Lois, G., Lemaitre, A. & Carlson, J. M. 2005 Numerical tests of constitutive laws for dense granular flows. *Phys. Rev.* E **72**, 051303.

Luding, S. 2001 Global equation of state of two-dimensional hard sphere systems. *Phys. Rev.* E **63**, 042201.

Lutsko, J. F. 1996 Molecular chaos, pair correlations, and shear-induced ordering of hard spheres. *Phys. Rev. Lett.* **77**, 2225–2228.

Lutsko, J. F. 2001 Velocity correlations and the structure of nonequilibrium hard-core fluids. *Phys. Rev. Lett.* **86**, 3344–3347.

Lutsko, J. F & Dufty, J. W. 1986 Possible instability for shear-induced order-disorder transition. *Phys. Rev. Lett.* **57**, 2775–2778.

Mitarai, N. & Nakanishi, H. 2005 Bagnold scaling, density plateau, and kinetic theory analysis of dense granular flow. *Phys. Rev. Lett.* **94**, 128001.

Mitarai, N. & Nakanashi, H. 2007 Velocity correlations in the dense granular shear flows: effects on energy dissipation and normal stress. *Phys. Rev.* E 031305.

Orpe, A. V., Kumaran, V., Reddy, K. A. & Kudrolli, A. 2008 Fast decay of the velocity autocorrelation function in dense shear flow of inelastic hard spheres. *Europhys. Lett.* **84**, 64003.

Pouliquen, O. 1999 Scaling laws in granular flows down rough inclined planes. *Phys. Fluids* **11**, 542–548.

Reddy, K. A. & Kumaran, V. 2007 The applicability of constitutive relations from kinetic theory for dense granular flows. *Phys. Rev.* E **76**, 061305.

Sela, N. & Goldhirsch I. 1998 Hydrodynamic equations for rapid flows of smooth inelastic spheres, to Burnett order. *J. Fluid Mech.* **361**, 41–74.

Silbert, L. E., Ertas, D., Grest, G. S., Halsey, T. C., Levine. D. & Plimpton, S. J. 2001 Granular flow down an inclined plane: Bagnold scaling and rheology. *Phys. Rev.* E **64**, 51302.

Silbert, L. E., Grest, G. S., Brewster, R. E. & Levine, A. J. 2007 Rheology and contact lifetimes in dense granular flows. *Phys. Rev. Lett.* **99**, 068002.

Stevens, M. J. & Robbins, M. O. 1993 Simulations of shear-induced melting and ordering. *Phys. Rev.* E **48**, 3778–3792.

Theodosopulu, M. & Dahler, J. S. 1974*a* Kinetic theory of polyatomic liquids. I. The generalized moment method. *J. Chem. Phys.* **9**, 3567–3582.

Theodosopulu, M. & Dahler, J. S. 1974*b* Kinetic theory of polyatomic liquids. I. The rough sphere, rigid ellipsoid and square-well ellipsoid models. *J. Chem. Phys.* **9**, 4048–4057.

Torquato, S. 1995 Nearest neighbour statistics for packings of hard disks and spheres. *Phys. Rev.* E **51**, 3170–3182.